D5.3

Dissemination report on structured illumination demonstrator results

Project number	101014977
Project acronym	REALHOLO
Project title	Phase modulating micro mirror array for real holographic mixed-reality displays
Start date of the project	1st January, 2021
Duration	60 months
Call	H2020-ICT-36-2020

Deliverable type	Report
Deliverable reference number	ICT-36-2020 / D5.3 / 1.0
Work package contributing to the deliverable	WP5
Due date	December 2025 - M60
Actual submission date	7th January 2026

Responsible organisation	HOLOEYE
Editor	Hagen Stolle
Dissemination level	PU
Revision	1.0

Abstract	Developments of optics for use with MEMS-SLM are presented with absolute data and in comparison to prior art SLM. Distinguishing features as crosstalk elimination and high-speed de-speckle methods are used to show the great potential of MEMS-SLM .
Keywords	MEMS-SLM, PLM, Phase modulation, Holography, Diffractive optics

PHOTONICS PUBLIC PRIVATE PARTNERSHIP

The REALHOLO project has received funding from the European Union's Horizon 2020 research and innovation programme under grant agreement No. 101014977. This project is an initiative of the Photonics Public Private Partnership.

Editor

Hagen Stolle (HOLOEYE)

Contributors (ordered according to beneficiary numbers)

Max Liebmann, Tobias Reusch (HOLOEYE)

Disclaimer

Executive Summary

This report summarizes highlights of the setup, use and performance of demonstration systems designed to investigate selected features of the new type of MEMS-SLM developed within the scope of REALHOLO. It includes background on the motivation to focus on certain measurements and references their relevance to SLM characterization in general. Accordingly, several SLM types were deployed. This approach not just made the development and validation process more efficient, it also helped to ensure general applicability of the solutions as well as their robustness.

As planned, work focused use-relevant aspects of characterization as well as pattern generation. This means for instance that measurements should provide precise results but with robust and simple to use setups and procedures. Different types of patterns ranging from basic binary gratings to more complex holographically reconstructed images were used.

The implementation and completion of setups and procedures was somewhat hindered by delays in delivery of final REALHOLO MEMS-SLM hardware but work-arounds were found for the analyses and interpretations. Comparing results from the various hardware platforms, feature expectations for MEMS-based SLM could be analysed and confirmed which further supports the bright outlook on mirror-based phase SLM in use case fields where they can most contribute as:

- Short wavelengths reliability (sustainability to high intensity UV)
- High speed (frame rates of >= 1 kHz)
- Polarization independence (increased light efficiency)
- High spatial frequencies (high resolution holograms without crosstalk and image noise)

In an effort to accelerate system development and integration with real life use cases, once MEMS-SLM TRL will have matured sufficiently, an exemplary optics design is presented to demonstrate a representative option for a space-efficient projection system. It features a compact RGB laser-illuminated optics to further magnify the diffraction angle given by the physical pixel size of the SLM into a large angular region of interest - one large diffraction order, for many types of content.

Application of the fast response and high frame-rate of the MEMS-SLM, one of it key features, is validated in a de-speckling solution. The fast and precise MEMS modulation directly enables time-integrated solutions, where not simply speed is of importance but also high bit depth of high spatial resolution phase patterns (holograms) which in turn enables deterministic methods relying on low crosstalk phase modulation.

Table of Content

List of Figures

List of Tables

Chapter 1 Introduction

The new generation of MEMS-SLM developed in REALHOLO is used in laboratory-type setups to test selected key characteristics which are representative for use in holographic AR and other high frame-rate multi-wavelength applications. Tests are conducted in monochrome and with coherent RGB illumination.

Investigations of use case-relevant aspects are done with colour-field-sequential (CFS) optical systems which ensure robust use (without side effects with impact on interpretation of results), flexible integration (for potential adjustments) and easy operation (efficient use). In order to support the desired analyses but also prepare for higher integrated setups as the projection engine, dedicated lab setups included considerations as:

- Ability to optically combine and synchronize multiple light sources and signal patterns in a spatially and temporally super-positioned single wavefront or holographic reconstruction
- Ability to address and characterize diffraction patterns with general importance to structured illumination, coherent wavefront modulation as well as holographic AR
- Ability of principle verification of quality aspects as
    - Zero order diffraction efficiency (DE),
    - DE of higher DO (diffraction orders),
    - Background noise between DO
    - Contrast in a holographically reconstructed image pattern
    - Super-positioning of multiple wavelengths, e.g for full colour RGB

In order to demonstrate the importance of appropriate design for diffractive (or holographic) applications, a diffractive projection engine (DPE) is shown as exemplary implementation. Its compact implementation is representative for robust and compact integration of coherent multi-wavelengths illumination with high-resolution optics of large numerical aperture.

A de-speckle method for significant reduction of interference noise from coherent illumination combined with holographic image generation is presented, which greatly benefits from advanced features of the new REALHOLO MEMS-SLM, as high frame-rate, high bit-depth and low inter-pixel crosstalk.

Chapter 2 Design and preparation of SLM tests

Systems for, expertise and experience in characterization of high-resolution microdisplays is available in the consortium in the full range from manufacturing-driven test to application-relevant characterization and evaluation in actual use. While work package 3 (and corresponding deliverables) focuses on device properties, work package 5 focuses on use of the device and characterization with setups and procedures which are robust and simple to use.

Challenges resulted from the required adaptation and scale-up of existing measurement setups and routines originating from LCOS investigations, to some degree from the limited functionality of test samples, but also from their temporal characteristics in the kHz regime and necessary universal CFS laser timing/driving. Different measurement setups were adapted individually; some key efforts are described her but more elaborated in the chapters below.

As described elsewhere in general MEMS-SLM characterization, we had to implement nitrogen purging for the early generation of MEMS based SLM chips to ensure their survival of and proper performance in regular lab use. This effort included several practical challenges but in the end it proved a valuable enrichment for future sampling and projects.

Already available measurement software is designed to operate LCOS devices using a proprietary software development kit (SDK). Due to automation, even complex measurement routines can be handled without an operator. As part of this project, we integrate various individual SLM functionalities into the existing environment.

In addition, most of the existing setups are limited to operate actively controllable samples. Well-defined and properly driven reference patterns are required to ensure smooth operation and automated evaluation, especially in tests were regions on the SLM act as a reference themselves. Therefore, in some cases we have to adapt the way we interpret results, and sometimes we have to (temporarily) use equivalent hardware replacements (non-REALHOLO devices but representative substitutes) to demonstrate new features of the test systems or of the future devices.

Since LCoS based SLMs have their switching time limits, test systems are tailored to frame rates of 60-180 Hz. Therefore, system upgrades also included signifiant resources for the proper triggering of light sources of different kinds for the new kHz target. Of key importance are temporal properties as laser switching speed and stability because they may directly lead to wrong conclusions about the MEMS characteristics. Result of the corresponding selection process was the *FISBA READYBeam* (TM ind 2 1007773), which proved to be suitable for the systems requirements, with its digital modulation frequencies of 1 MHz and its digital rise/fall time 10/90% of 11 ns.

Figure 1: Fisba READYBeam [1].

Interfacing active components of our setups was supported by an universal lab-style laser trigger box which was made for the project and is used to synchronize frame change signals with laser trigger signals for each colour (RGB). It also provides a BIAS voltage to drive SLM pixels with proper voltage levels which correspond to the triggered laser colour. An FPGA board can set multiple driving schemes and parameters as:

- Frame rate
- Number of bit planes after trigger
- Pattern sequence mode (R,G, B, R, G, B, ...) or (R, R, ..., G, G, ..., B, B, ...)
- Laser delay
- Laser active time
- Voltage level for BIAS for different colour fields (e.g. R, G, B)
- Laser voltage levels (low, high)

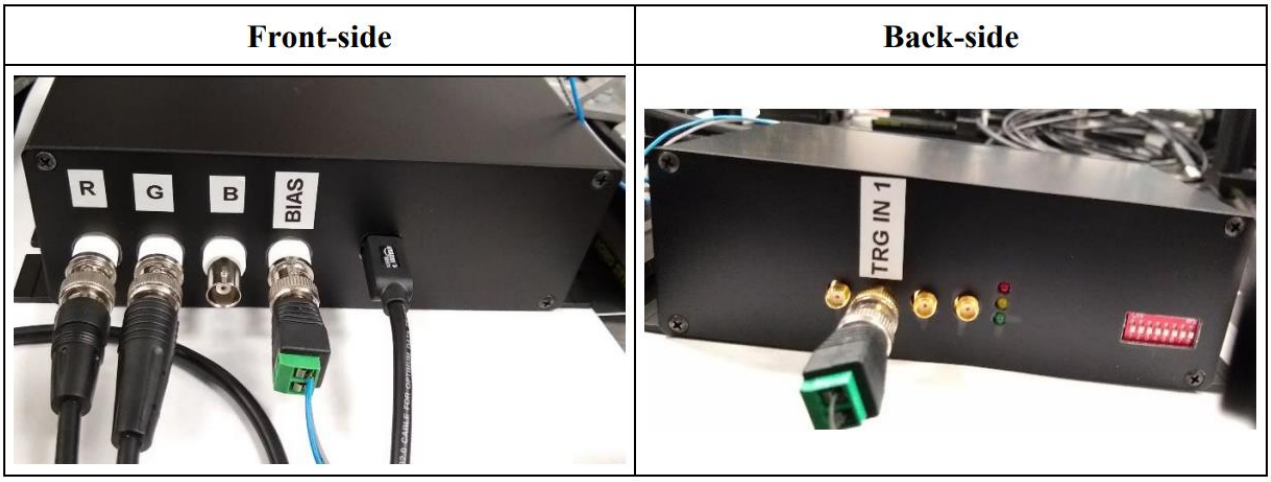

Figure 2: Universal laser trigger box.

Chapter 3 Tests and evaluation - PHS

In this chapter we want to focus on application-oriented scenarios. In order to assess the REALHOLO MEMS-SLM relative to other SLM technologies, it is essential to investigate its performance as well as its potential limitations in everyday use cases. Due to prior experience with LCoS-based modulators, we are very much aware of common characteristics as polarization dependence or temporal behaviour, all of which are expected to improve for piston mirrors. Another relevant topic is crosstalk, which is an effect caused by adjacent pixels interfering with their neighbours. This effect is more noticeable with high spatially frequent phase functions than for smooth continuos ones. Accordingly, we use regular binary grating functions with spatial variations and monitor their corresponding diffraction efficiencies to visualize crosstalk effects.

In contrast to binary gratings for symmetric diffraction in plus and minus orders, blazed phase functions are important for high-efficiency beam steering in only one direction. In the ideal case these functions would be represented by a continuos phase ramp. Once the phase would exceed a value of 2PI, there will be a phase wrap back to zero level, hence called 2PI modulo. In addition, the pixelation of SLMs causes discrete phase steps that can have an impact on the diffraction efficiency. On the other hand, crosstalk effects as found in LCoS may have a positive (“smoothing”) effect by reducing or suppressing phase steps.

In this chapter we present a proprietary camera setup to measure diffraction efficiency of various patterns addressed by the passive (hardwired) holo SLM (PHS), which will also serve other SLM types. The measurement results of binary and blazed gratings will be discussed with respect to a LCoS-based SLM reference.

3.1 Diffraction efficiency - Setup

The diffraction efficiency is determined by the intensity of the diffracted spot in relation to either the total input or the reflected non-modulated output power. This can be done with a conventional power meter, but it would be a tedious task once you look at more than one pattern or at multiple diffraction orders resulting from a structured phase pattern. In addition, one has to keep a number of things in check: power meter calibration and angle dependency, aperture position for spatial filtering and efficiency of procedures. Therefore, we went with a camera-based setup. The camera of choice is the G2-1600 Moravian (G2-Mark II) with sensor type KAF1603 CCD and is commonly used in astronomy to capture stars, because of its excellent linearity and high dynamic range. This makes it the perfect fit for reliable power measurements across a range of diffraction orders of varying intensity and represents the heart of the setup.

Due to the common 50:50 beam splitter configuration for reflective SLM, we can ensure zero degree input angle onto the SLM. A mirror is placed in the second optical path that acts as a constant reference spot on the camera regardless of the SLM modulation or laser power fluctuations. It will be the baseline for all calculated diffraction efficiency values.

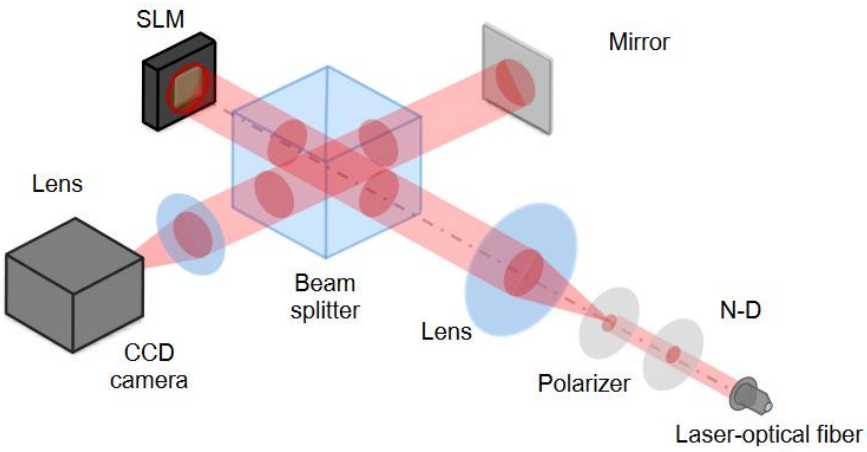

Figure 3: Setup sketch of the diffraction efficiency camera setup.

The chosen lens configuration in front of the camera collects diffraction angles of up to ~10°, which is sufficient for binary 1-1 gratings with pixel pitch of 4µm or higher, i.e. the highest spatial resolution of our systems.

Figure 4: Diffraction efficiency camera setup with PHS.

Illumination of the SLM variants for DE characterization is done with a collimated laser with 660 nm wavelength. While the multi-colour use cases deploy RGB laser sources, DE measurements can be done with a single wavelength and interpolation of data to other wavelengths as needed.

3.2 Diffraction efficiency - Binary gratings

Characterization of device-related efficiencies is best performed with discrete and regular patterns since results from more complex phase patterns, as in image holograms, will also incorporate potential effects from type and quality of hologram computation and encoding.

Binary gratings represent an ideal case for evaluation of device performance. If mirror arrays in MEMS-SLM are very homogeneous in their response to electrical signals, they can represent their theoretical equivalent quite precisely. Simplicity of binary gratings reduces the sensitivity to errors but still generates data to evaluate various effects ranging from absolute diffraction efficiency to potential asymmetry of modulation for different physical orientation of a device or for temporal effects. Binary gratings have their largest efficiency for a modulation of 1Pi (a half wave). If phase modulation is further increased by a device capable of more than 1Pi, efficiency starts to drop again. This is an effect that can also be used as a feature if there are no other measurement systems available, e.g. for determining the required voltage for 1Pi or 2Pi modulation. In case of an ideal binary grating, i.e. not potentially disturbed by discontinuities from other patterns as separations in a pixel array, the normalised efficiency of diffraction into the first and zero orders of a sufficiently coherent wavefront looks as shown in Figure 5; higher orders are ignored for simplicity. Intensity in the zeroth order drops as the plus and minus first orders increase; the image shows them added in the orange line.

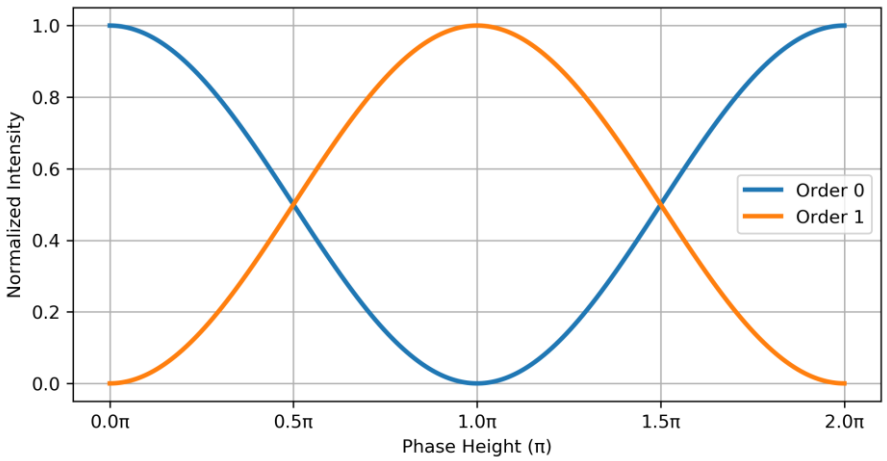

Figure 5: Normalized intensity of diffraction order 0 and 1 (sum of minus and plus order) over the phase scaling of an ideal binary grating.

Reference to comparable measurements with LCoS-SLM

One aspect of the original motivation for MEMS-SLM development is independence of individual pixel modulation from adjacent pixels. If realised perfectly, this leads to very “clean” and predictable modulation of coherent wavefronts, where clean means that elimination of modulation artifacts significantly reduces undesired diffraction effects as higher diffraction orders or scatter loss.

In liquid crystal-based SLM, interaction between adjacent pixels is always present in high spatial frequency applications, in our current discussion this would be binary 1:1 gratings with the smallest possible pitch of 2 pixels. The effect in LCoS is amplified if the ratio of pixel size (i.e. pitch) relative to the LC cell gap (LC layer thickness) is small. Since phase modulation in LCoS is generated by the birefringence of the LC material which in turn is limited by chemistry, there exists an inherent problem with modulating light of long wavelengths with SLM with small pixels. The discussed ratio always tends to be high for high-resolution SLM and interaction between neighbouring pixels will be noticeable as result of electrical field distribution and LC material viscosity, so-called fringe effects, which is a type of inter-pixel crosstalk. Figure 6: below shows fringe effects for a LCoS with small pixel pitch configured for a long wavelength (~1500 nm). The red line represents the phase retardation which ideally should be a rectangular-shaped binary grating with the same pitch as the SLM matrix.

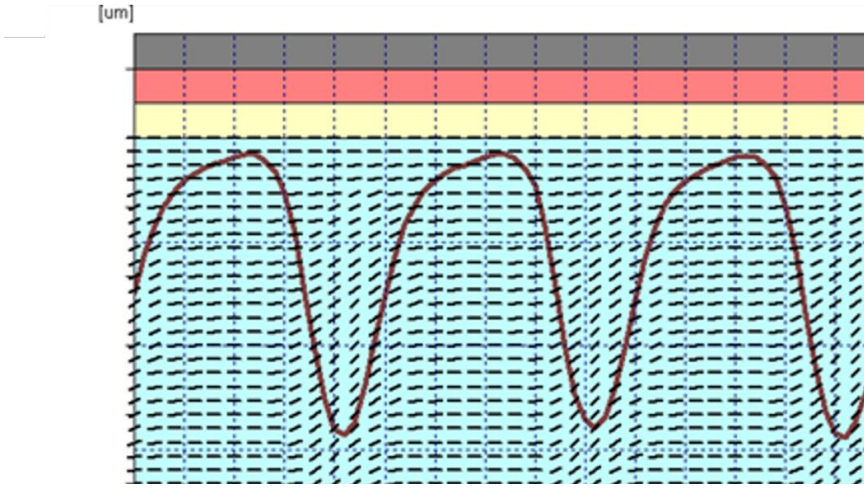

Figure 6: Phase retardation of LCoS layer with 1:1 Binary grating.

While fringe effects in LCoS are to be expected for high spatial resolutions, also for larger virtual grating pitches the transition of retardation between adjacent pixels of greatly different pixel voltage and corresponding field strength impacts on the modulation quality. This can be seen in Figure 7.

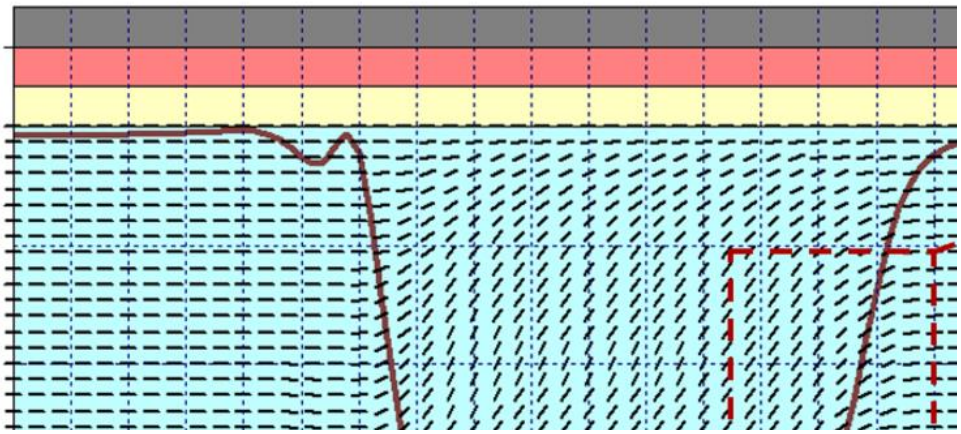

Figure 7: Phase retardation of LCoS layer with 4:4 binary grating, highlighted transition zone from LC fringing.

As mentioned above, LC fringing leads to undesired diffraction effects as higher diffraction orders or scatter loss which are potentially amplified by unfavourable pixel pitch-to-cell gap ratios. The resulting loss of diffraction efficiency cannot only be seen in the desired first (or higher) diffraction orders but more easily in the zero order. The more light is deflected into the higher orders, the less intensity remains in the zero order. Since binary gratings have their peak efficiency at 1Pi, no light should remain in the zero order at that value. Now, if a certain grating pitch exhibits less efficiency as result from fringing, effective LC modulation to 1Pi takes more voltage to overcome the restrictive forces in the LC layer. This can be seen below in Figure 8 and Figure 9 below. In Figure 8 an LCoS-SLM with larger pixels (and more favourable ratio of pitch and cell gap) exhibits rather similar behaviour for different virtual grating pitches. 1Pi modulation is reached approx. at grey (or voltage) level 120. But even at this larger pitch it can be seen that when voltage is further increased to 2Pi (approx. voltage level 256 = 8bit) the larger pitch reverses back to full intensity in the zero order more quickly than smaller pitches. For an ideal grating, 0Pi and 2Pi represent the same phase value. In a real binary grating this would require a perfectly flat step-wise pattern of pixels with 0Pi and pixels with 2Pi. But as an effect of LC fringing, as visible in the phase profile in Figure 7, 2Pi values differ from ideal. The fact that none of the three virtual gratings in Figure 8 below fully return to full zero order intensity is a result of this imperfection and more pronounced for smaller pitch gratings.

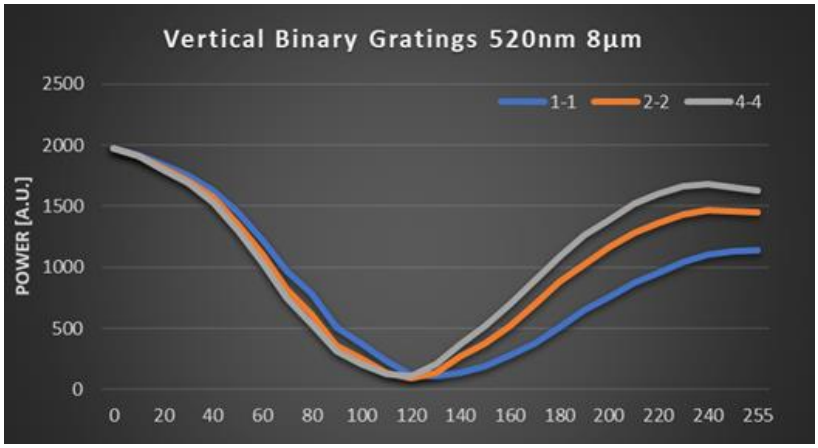

Figure 8: Power of zero order binary grating of 8 µm pixel SLM at 520 nm for different grating periods.

The effects of grating imperfections from LC fringing or crosstalk are stronger for smaller pixels, which can be seen in Figure 9. Not only is more voltage required to achieve a 1Pi grating for high spatial resolution but also zero order intensity at 2Pi is lower than for larger pixels, which can be seen well when comparing e.g. a 2:2 grating for 8 µm pitch with 2:2 for the 3.74 µm SLM.

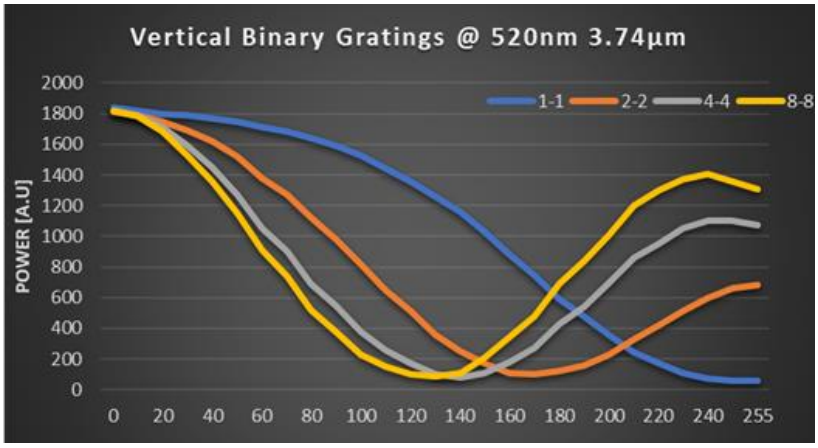

Figure 9: Power of zero order binary grating of 3.74 µm pixel SLM at 520 nm for different grating periods. Strong crosstalk effect noticeable.

As mentioned before, side effects from the viscous LC material in combination with cell geometry and electrical field distribution may cause further imperfections in high-resolution phase modulation beyond crosstalk. One example is LC alignment relative to substrate surfaces (glass, Silicon) where proper LC modulation requires an angle offset from parallel in order to generate some “stress” in the LC for better response to the electrical field. This offset in orientation of LC molecules is called “pre tilt”. The asymmetric LC orientation also causes a small asymmetry in 1st and minus 1st order for certain grating orientations. Use of MEMS-based SLM is aimed at eliminating such LC-related effects.

Measurement of binary gratings using PHS

The protective Nitrogen purge hood for the passive i.e. hard-wired MEMS-SLM “PHS” (passive holo SLM) exists in variants with and without optical window. A window is preferred to avoid potential contamination of the sensitive mirror array but light reflections from or interference with the window may create undesired effects. Potential interferences may be reduced by use of lasers with short coherence length. But in our setup, the cover glass of the purge hood was tilted slightly out of the ROI. That way reflections do not interfere with the diffraction orders directly, but still there will be some light reflected back reducing the signal levels in comparison to the reference mirror spot.

Reference is taken to explanations above in this document on how measurement of the zeroth and first diffraction orders can be used to interpret certain effects. It should also be noted again that elaborate testing and evaluation of the actual devices was performed and reported earlier. Measurement systems and procedures for use case relevant tests were developed and validated with a range of SLM. PHS are also used to prepare everything for fully controllable AHS and to support the the dialogue with Fraunhofer IPMS and RealView on device properties and use scenarios.

The hard-wired structure of PHS with most regions (of the same design properties) of only Millimetre size or below require precise alignment with measurement setups but still with increased the risk of artifacts from edge effects or overexposure into neighbouring structures. While this is of no concern for full-resolution tests as TGI, it may impact on measurement of diffraction effects where it is not directly obvious if additional pixels contribute, especially since even in good/desired regions not all pixels may work properly yet. But work with PHS and other SLM was well suited to demonstrate the capabilities of the systems and the interpretation of results.

Similar to reference work with LCoS showing the transfer of light/intensity from the (non-diffracted) zero order to the desired first order(s), application of virtual gratings of different pitches to PHS showed the same expected effect: the zero order intensity drops and the first order intensities increase up to 1Pi and reverse for higher phase values. Since in the newly developed measurement systems a physical intensity reference exists from the additional mirror, efficiencies don't have to be normalised to 100% but can be measured at their absolute values, as seen on the y-axis.

Selected results shown in Figure 10-13 below show that the PHS shows good agreement with the expected characteristics. Following the zero order plot in Figure 14 we can define where the phase level is reaching 1Pi (6.6 V) and 2Pi (7.6 V) by looking at the local extremes. However, the modulation is not as pronounced as we see with higher TRL LCoS devices, only reaching a minima of around 10% from the initial 50%. Additionally the maximum of the zero order at 2Pi is just short of the initial value with 35-40% DE. Most noticeable (and very positively received even for this early sample) is the fact that there is no movement of the extrema along the x axis, which has been a clear indicator for crosstalk with LCOS. Only the suppression of the zero order not reaching is global maximum again could lead to the conclusion of existing interaction of adjacent pixels but may also be a result of imperfect switching or orientation of some broken pixels.

Looking at the first orders of the binary gratings we could see that the symmetry of the positive and negative order is dependent on the grating period. We know asymmetric behaviour from LCoS devices due to their pre-tilt of the crystals. Pre-tilt also causes phase modulation for parallel SLM orientation to differ from perpendicular orientation in the optical setup, leading to a different DE for vertical or horizontal orientation. That being said, in LCOS this can be considered in the orientation of the grating relative to the physical device. In our PHS tests the asymmetry seems to be arbitrary valid for period 1 and 8, while periods 2 and 4 show great symmetry. However, we see no such correlation of grating period for the sum of first DO nor zero order respectively. This can be seen as a great indicator for a very weak crosstalk effect, if any.

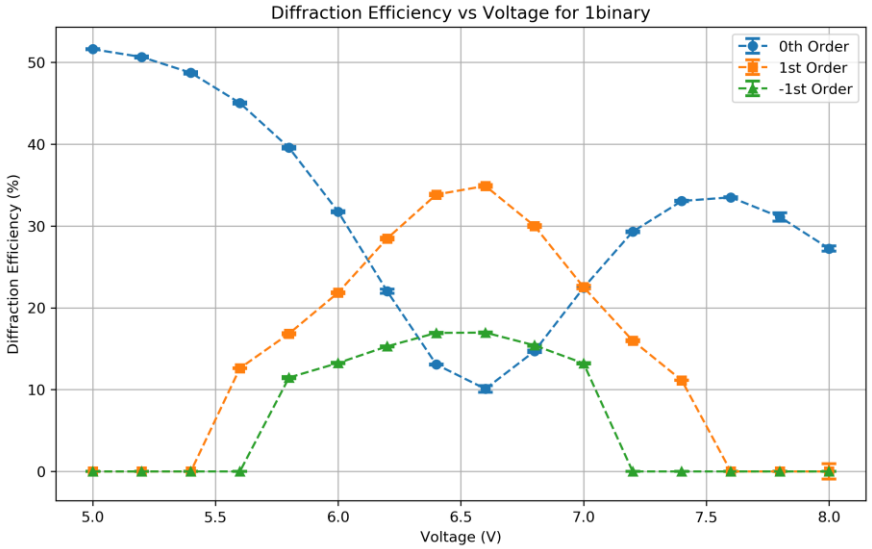

Figure 10: PHS diffraction efficiency over voltage of a binary grating with period 1:1 at 660 nm.

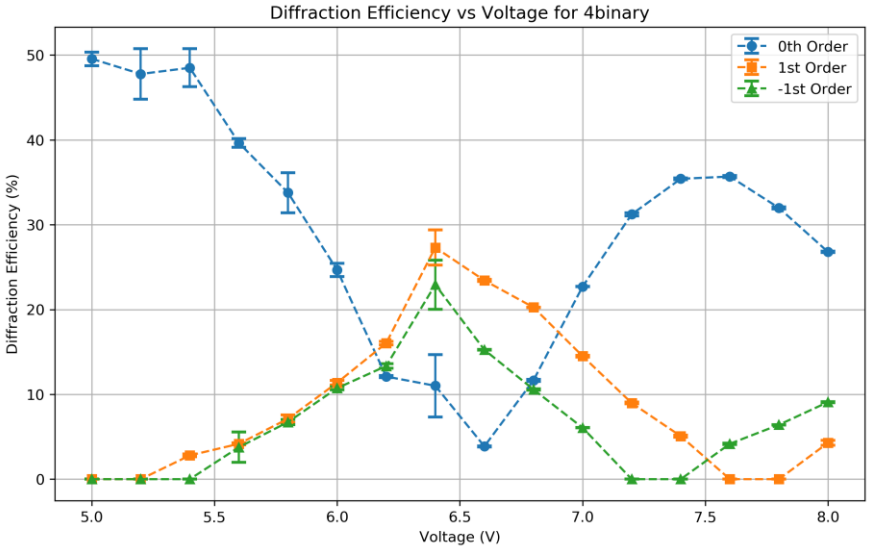

Figure 12: PHS diffraction efficiency over voltage of a binary grating with period 4:4 at 660 nm.

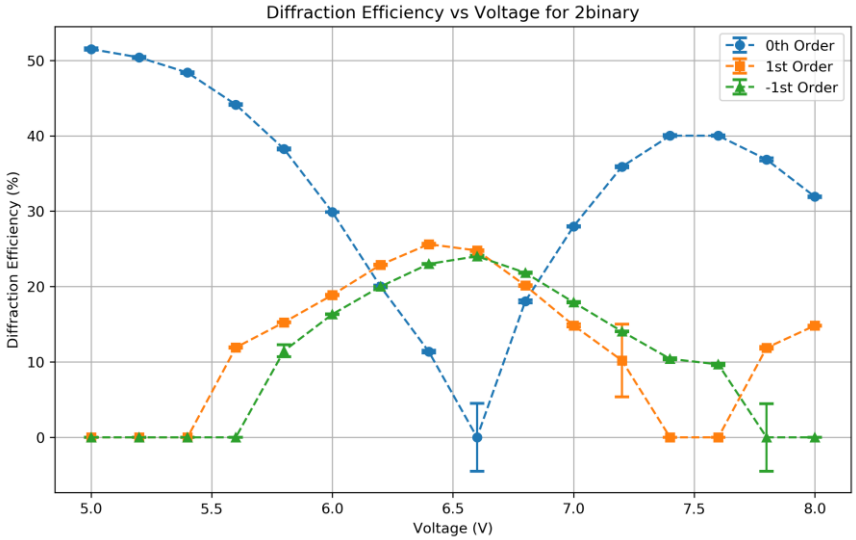

Figure 11: PHS diffraction efficiency over voltage of a binary grating with period 2:2 at 660 nm.

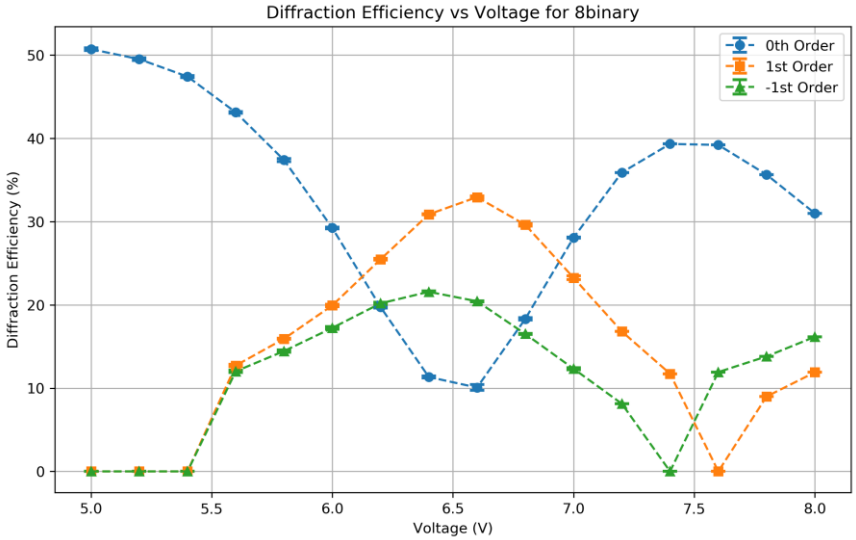

Figure 13: PHS diffraction efficiency over voltage of a binary grating with period 8:8 at 660 nm.

While qualitative response of the PHS matches well with expectations, albeit imperfections of the global array as well as a number of individual mirrors, and even quantitative data is in the proper range, an asymmetry can be seen when voltages are increased beyond 1Pi and zero order intensity should return to full value. In MEMS-SLM of final TRL this should be the case to a very large degree, maybe not 100% but close. In this earlier state of development hardware, several reasons contribute to this effect of reduced 2Pi efficiency:

- Pixels not working at all (bias/phase offset both at 0Pi and 2Pi and wrong at 1Pi)
- Pixels not achieving full stroke (potential phase offset at various grey values)
- Pixels with slight mirror tilt (angular deflection shift relative to ROI)

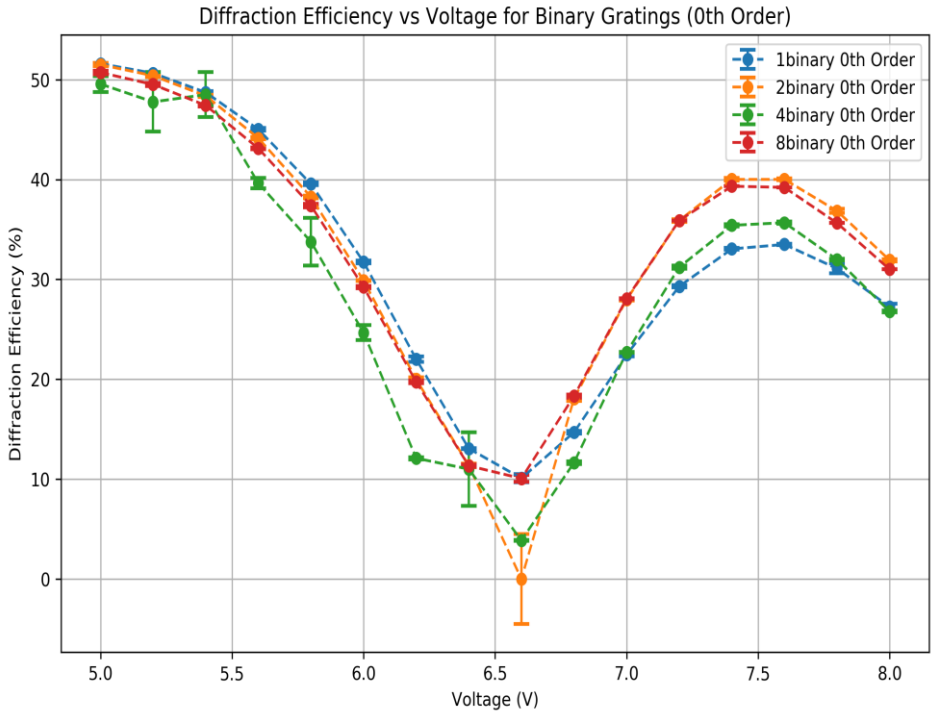

Figure 14 PHS zero order diffraction efficiency over voltage for number of different binary grating periods

3.3 Diffraction efficiency - Blazed gratings

Another commonly used function is the blazed (or sawtooth) grating, similar to other beam steering or shaping functions like the Fresnel lenses, axicons, vortex phases. This type of content operates in a phase regime of 2Pi modulo and only features a few discrete phase jumps (one each tooth), while the rest of the function consists of continuos/smooth ramps. Therefore the crosstalk, as visible in high spatial frequency (small pitch) binary gratings, becomes less noticeable. However, due to the pixelation of SLMs, continuos phase ramps become quantized leading to non-ideal efficiency. Increasing the number of pixels per blazed grating period decreases the impact of the quantization effect but increases the grating pitch. So it is obvious that by decreasing the number of pixels per period the phase function will diverge back to a binary 1x1 with two discrete phase steps after all.

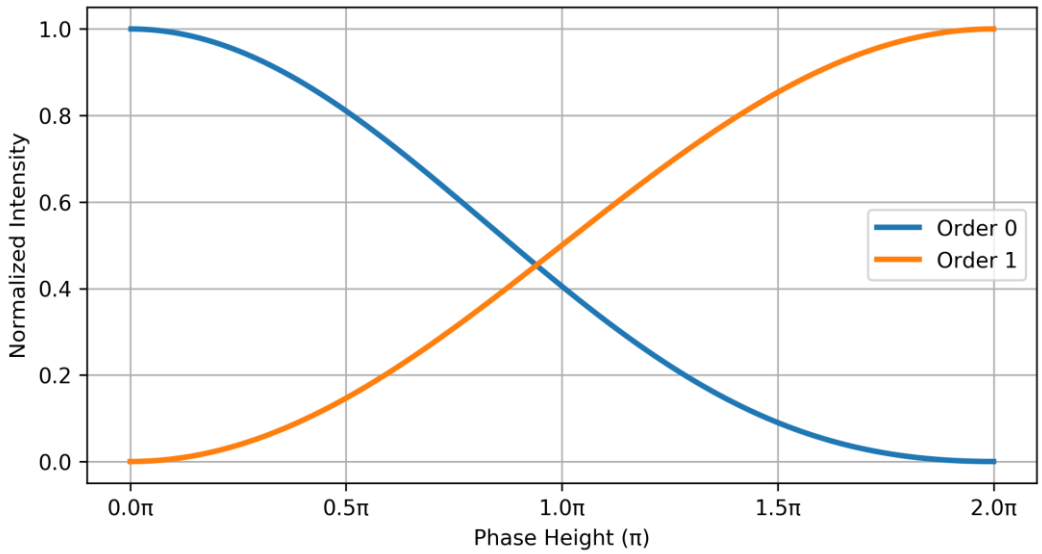

Figure 15 Normalized intensity of diffraction order 0 and desired 1 over the phase scaling of an ideal blazed grating without quantization

Typical test patterns used for LCoS are 8-period and 16-period blazed gratings. Conveniently, this is what the PHS samples are designed to do on segments S7-S9. In the title of the diagrams below, UP refers to a positive phase ramp (equivalent to 1st order binary position), while DOWN refers to a negative phase ramp (equivalent to minus 1st order binary position).

In case of the PHS, the results are plotted in Figure 16-19 for 8 and 16 in both directions. The characteristic shape of DE with phase scaling compared to the theory is represented. Unlike the binary gratings, here we see a strong difference between the different grating periods. In case of the 16 period grating the zero order pushes a minimum DE of under 5%, which is quite good considering the pixel yield of early PHS. One can notice that there is another asymmetry between positive (UP) and negative (DOWN) ramp direction. This is consistent for both grating periods, while the 8pitch grating is performing worse overall. Even though the binary grating showed no correlation of DE to grating period we can see a clear improvement here. Keep in mind that a blazed grating is much more dependent on a linear phase response. We did not perform an active linearization but simply worked in the linear regime of the physical response curve of the device, leading to a small divergence to the optimal configuration but on the other hand demonstrating the excellent design and manufacturing quality. In addition, we discussed earlier that the smooth phase function of the blaze can be better represented by discrete phase steps by simply increasing the number of steps. This greatly improves the performance of the 16 pixel grating.

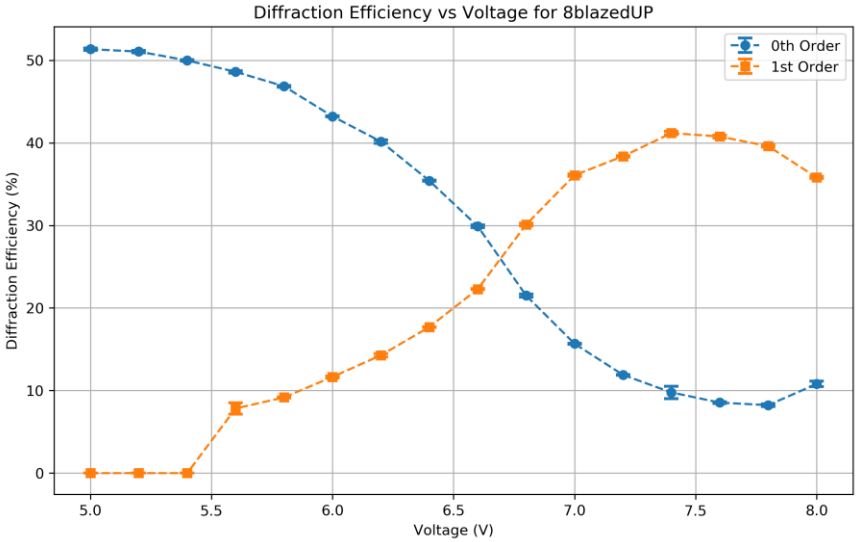

Figure 16: PHS diffraction efficiency over voltage of a blazed grating with positive period 8 at 660 nm

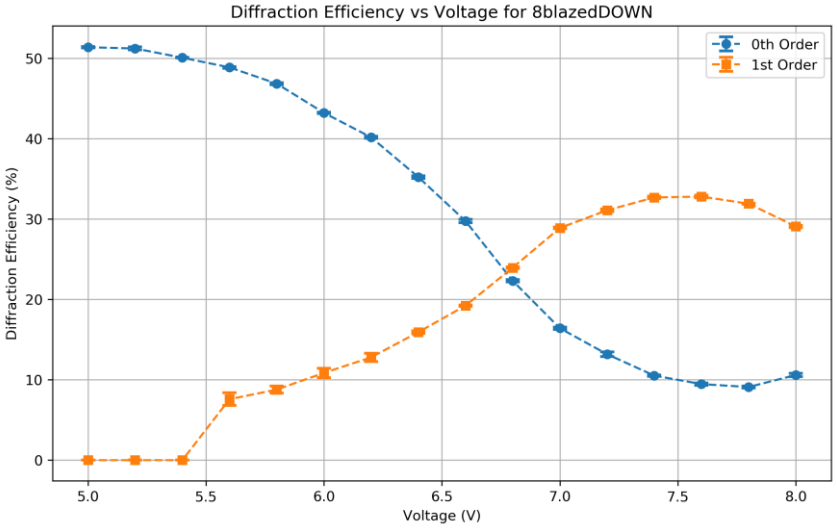

Figure 17: PHS diffraction efficiency over voltage of a blazed grating with negative period 8 at 660 nm.

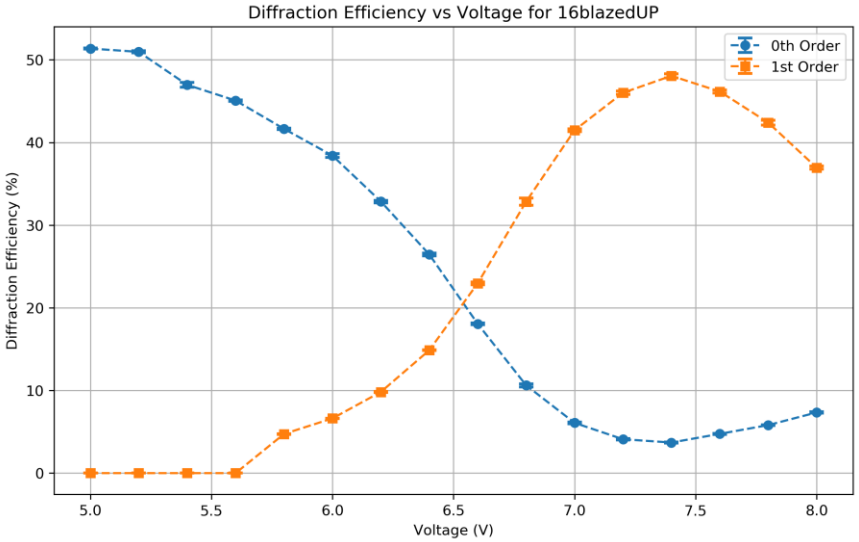

Figure 18: PHS diffraction efficiency over voltage of a blazed grating with positive period 16 at 660 nm.

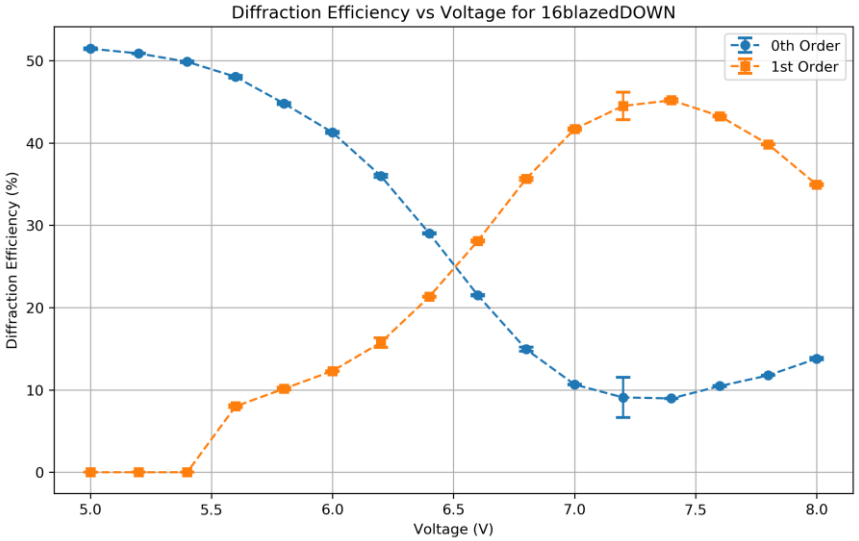

Figure 19: PHS diffraction efficiency over voltage of a blazed grating with negative period 16 at 660 nm.

3.4 Temporal behaviour

3.4.1 Introduction to use of PLM as temporary substitute

Since the PHS capabilities in their current wiring are limited to line patterns in small regions, we looked for alternatives in case the AHS would not be available to HOLOEYE in time. We learned that there is an evaluation kit of a phase light modulator (PLM) by Texas Instruments (TI) available, so we decided to use the PLM and to support our preparations for the AHS with this piston-type modulator. There are key differences between the REALHOLO chip and the TI chip: TI groups a number of binary-switching transistors on their CMOS backplane to drive one mirror placed on top of this super-pixel in order to achieve several discrete phase steps. In their PLM they combine (2x2) four binary CMOS pixels to enable 4-Bit - 16 phase levels, which represents a limitation compared to the 8-Bit/10-Bit planned for the AHS. Another difference is the pixel size: The TI chip features pixel pitches of 10.8 µm which create a much smaller diffraction angle or ROI. Due to the super pixel approach the pixel pitch is directly linked to the phase level resolution, i.e. bit depth. If you would like to increase the number of phase levels you would have to bin more pixels, such increasing the super-pixel pitch even more. It should be noted that the number of CMOS pixels does only define the number of binary signals which can be activated under a certain super-pixel. They also impact on the bit-depth, meaning there might be fewer useable gray levels than the max. possible 16 due to the non-linear electro-optical response.

As result of the binning of CMOS transistors under larger super-pixel mirrors, the pixel number is reduced. The VIS 0.67 PLM sample used at HOLOEYE has a CMOS resolution of 2560 x 1600 binary sub-pixels, which translates to a final resolution of 1280 x 800 super-pixels. REALHOLO exhibits ~4000 x 2000 pixel resolution.

The packaging of the TI samples includes a cover glass. Addressing is done via Display Port with a frame rate of 60 Hz. 8-Bit RGB images are sent to address the binary pixels, but the content has to be custom-sorted each video frame due to the super-pixel logic. Important to understand is that the 8Bit depth of the source images do not refer to the phase bit depth of the phase pattern, which 4bit resolution is achieved by spatial use of 4 individual bits under each mirror. The 8-bit input resolution is used for temporal resolution i.e. time slots per colour. This means the PLM device can switch 8 times per colour channel per frame leading to a field rate of 1440 Hz = RGB x 8 x 60 Hz.

Figure 20: Texas instruments EVM 0.67” kit. controller board (left) and PLM board (right).

We use characterization of the PLM to validate our measurement routines in preparation for the AHS as well as to already investigate typical properties of MEMS-SLM with piston mirrors. For this we tested the temporal behaviour of the chip in conjunction with the triggered RGB laser and its timings. For comparison with the REALHOLO MEMS results, we measured the PLM DE for the optimized

phase stroke for various binary gratings (1, 2, 4 and 8) in vertical and horizontal direction. This again also serves for general evaluation of piston mirror MEMS-type SLM.

It was mentioned before that different types of setups where considered. At the start of the investigations, characterization was done with single photo-diodes which is cumbersome for effects spreading over multiple diffraction orders but is totally sufficient for other types of characterization. In fact, it may even be preferred due to its simplicity. We used this method for initial PLM characterization and found a confirmation of one of its key features: low inter-pixel crosstalk and good symmetry of diffraction. As can be seen below in Figure 21, the diffraction into the plus and minus first orders is very symmetric, in fact so much that the orange dot is right behind its blue partner. What can also be seen is a sensitivity to positioning the PLM vertically or horizontally in the beam path which indicates imperfections in this early PLM generation.

Since maximum DE of a binary grating is ~42%, there obviously was a mistake made during acquisition of DE for the highest spatial frequency of 1:1. But even with an offset of the absolute value, the positive symmetry statement still applies to one orientation in the optical path.

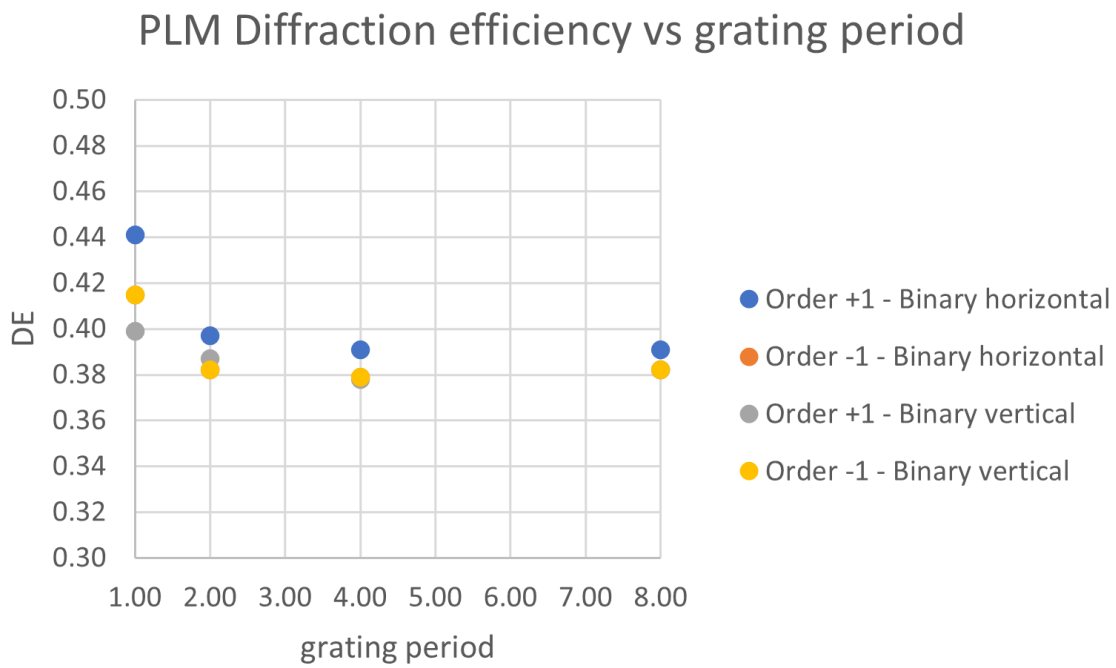

Figure 21: TI PLM diffraction efficiency for various grating periods for optimized phase stroke.

Summarizing these initial tests, it can be stated that mirror-type SLM can be evaluated similarly to their LC-based counterparts and that key features of MEMS-SLM are already visible with these tests.

Depending on the CMOS architecture and driving scheme, MEMS-SLM show a reset to zero (or less) in-between frames or sub-frames. These effects differ for the REALHOLO SLM and the TI chip and have to be considered during driving (e.g. duty cycle) and evaluation (camera timing). In its present configuration, the TI chip resets after each bit plane addressed for each sub-frame, i.e. the field rate of 8x compared to 60 Hz RGB. This is caused by the driving scheme, which forces the mirror back to its zero position before switching to the next phase level position, while loading the next phase data set. During that “off” state the BIAS voltage of the pixels can be switched if desired for multi-wavelengths operation. But in order to avoid misinterpretations from averaging across on/off cycles, the illuminating laser should be switched off for each sub-frame transition, i.e. 8x within each actual colour frame, and the camera should be synced. This is somewhat easier for the REALHOLO chip which is driven with constant phases within each colour frame. The TI chip creates more complicated driving because over the course of one frame with a standard integration time for example 16ms we need to trigger the light source more often. But in general, this must be done for any colour-field sequential device to ensure illumination in the on state only.

In this section we investigate the temporal behaviour of this phase reset of TI SLM by means of a fast photodiode to accommodate these high-speed effects in our measurements. Afterwards we reevaluate our common-path interferometer setup to enable phase measurements for high speed SLM devices. Although somewhat different, all of this is highly relevant to the REALHOLO devices and solutions can be directly transferred.

3.4.2 Rise and fall time - Photodiode

Temporal behaviour setup: Under a small incident angle, we illuminated the SLM with a collimated FISBA laser beam. The content, a simple grating, is addressed to separate zero and higher orders in the far field. A Si based photodiode type DET36A (rise time of 14ns) was placed into the order of interest. The power signal was visualized using a Keysight oscilloscope type DSOX2022A. The laser trigger signal from the universal trigger box was monitored to have reference point for the observed SLM modulation.

First we kept the chosen FISBA laser running in CW for red only and placed the photodiode into the position of the first order. As one can see, the photodiode signal has the shape of a square wave. The off-state, the time where the power is at its minimum and the on-state, the time where there is the power maximum, are clearly separable. However, the switch between both states is not instant. They have a characteristic shape that is unique to the mirror movement. Both rise and fall time are smaller than 50 µs. Worth noting is that the laser trigger signal only starts once the SLM is at its correct and stable position. Meaning the laser would only illuminate the actual pattern in the on-state, once we switch to a triggered mode. Those timings can be adapted via the laser trigger box FPGA program to match the individual SLMs characteristics.

As a complimentary measurement we also put the photodiode into the zero order. Showing the clear separation between off state and laser trigger signal once more.

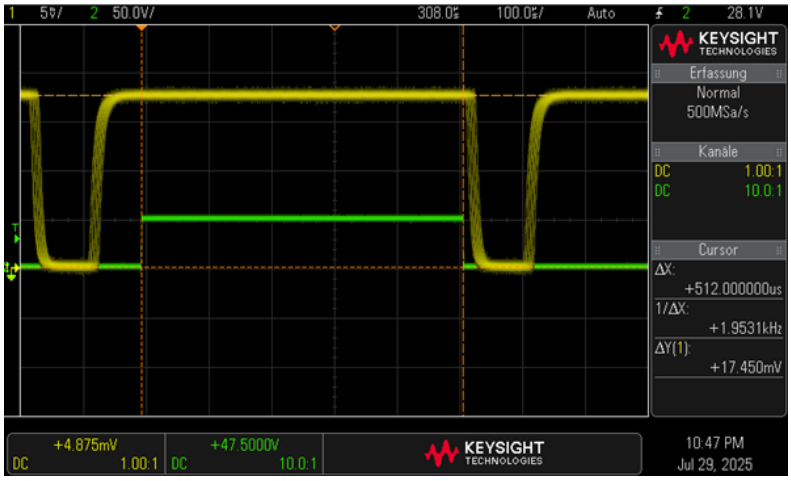

Figure 22: CW laser illumination: 1st order in yellow, red laser trigger signal in green.

Figure 23: CW laser illumination: 0th order in yellow, red laser trigger signal in green.

Since the laser was running constantly we could isolate the mirror movement characteristics. Another aspect to be tested was the triggering of FISBA laser via the red laser trigger output. Since we know the trigger signal is well isolated from the SLM movement we can look at the temporal behaviour of the laser source. The laser rise and fall time was specified to be 11ns which is even shorter than the photodiode resolution. So the only thing we can state for sure is that the laser response is fast enough to follow the laser trigger signal sufficiently and not interfere with the off state.

Figure 24: Triggered red laser illumination: 1st order in yellow, red laser trigger signal in green.

3.4.3 Common-path interferometer

Following up prior investigations with the photodiode, we wanted to evaluate the actual time-resolved phase modulation of high-speed SLMs. The TGI is not meant to measure time-resolved phase, since we need to take multiple images per phase level step to calculate the optical path difference. That is why we use another setup for high-speed tests: a common-path interferometer.

The idea is to have two light spots on the SLM to interfere with each other. By introducing small changes to one optical path by increasing the phase level, we generate a path difference that results in a movement of the fringe patterns. A camera can capture the fringes and their movement to calculate the phase in return. To achieve a high time-resolution, the setup is equipped with a line camera. As part of this project we integrated a new CCD into an existing setup. While the old camera only managed <30 kHz frame rate, the new Teledyne Linea 2k is able to capture in 52 kHz.

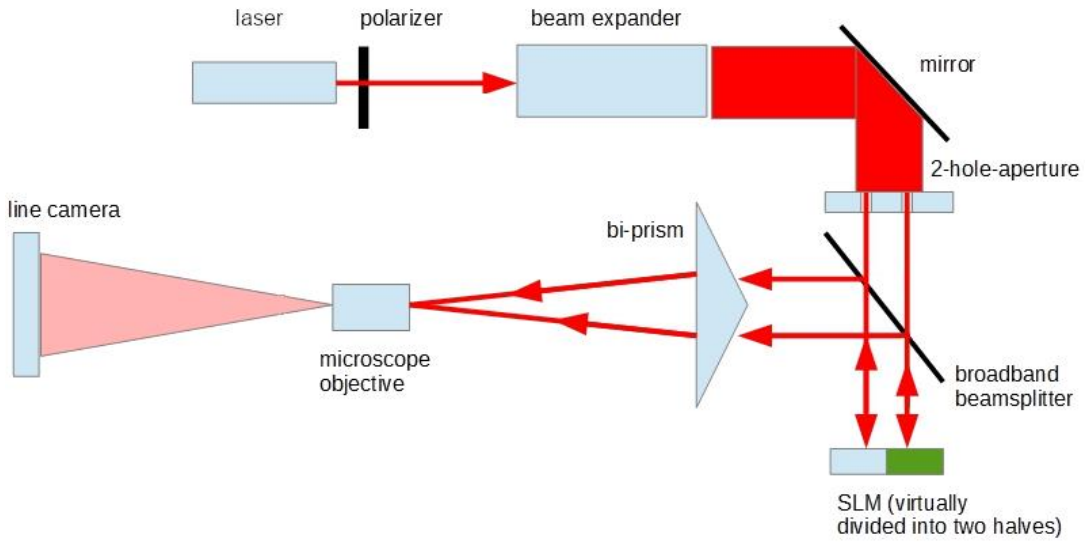

Figure 25:Common-path interferometer setup scheme.

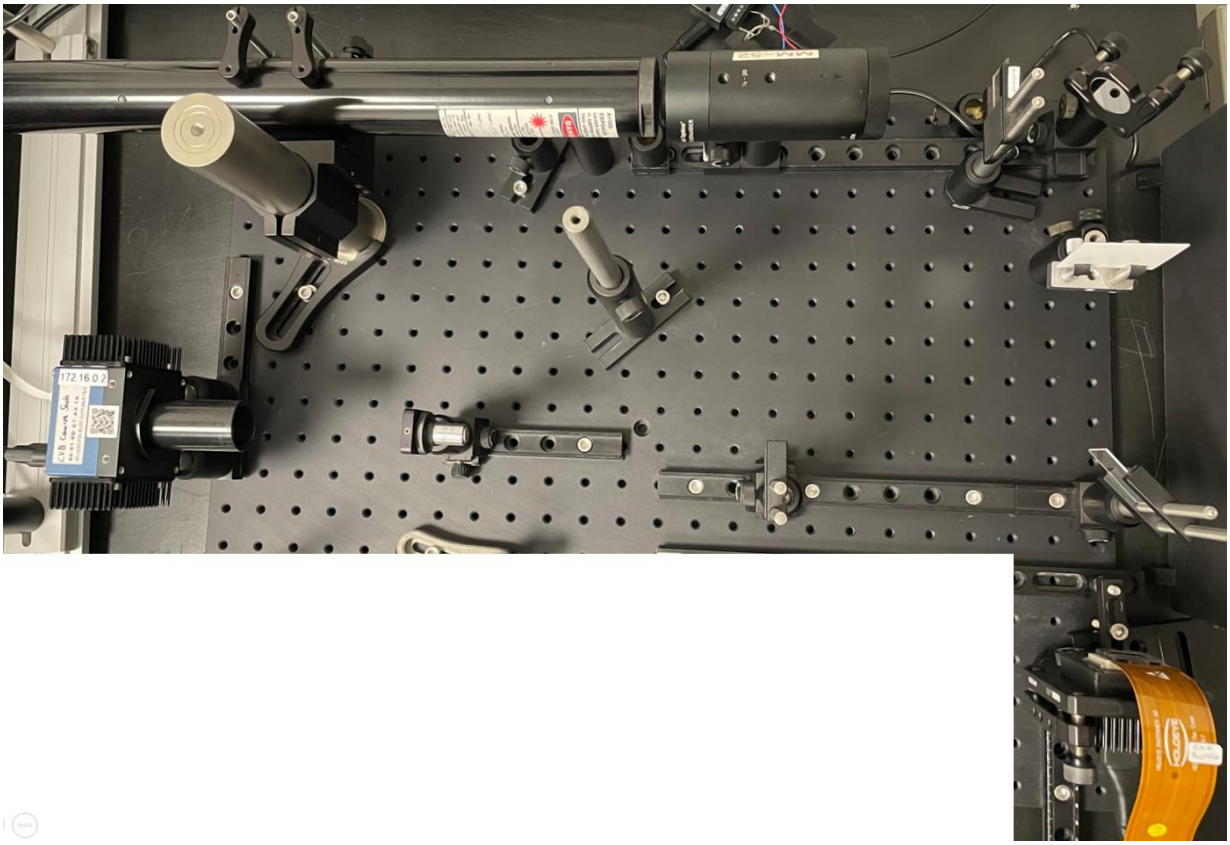

Figure 26: Common-path interferometer setup standard configuration with high speed line camera.

While one of the SLM halves acts a reference with constant zero level, the other half is driven with different phase values for each frame. The implication for the REALHOLO SLM is that the target bit depth of 8- to 10-bit has a clear advantage in order to realize a highly precise phase linearization and support many use cases. With such a high number of possible phase levels also the design space is much more forgiving and can be much more easily tailored to ones requirements.

3.5 Laboratory projection setup demonstrator

3.5.1 Introduction to the setup

This section is about a “breadboard-style” far field projection demonstrator based on MEMS systems. We will introduce the setup and continue with the CGH examples from single wavelength to RGB.

The projection demonstrator has many similarities with the diffraction efficiency setup described earlier. We have a collimator optic for the fibre-coupled light source. In this case it is reflective type to be wavelength independent, what will be important for RGB projection later on. The beam splitter is removed so that the setup has simplified beam path. Once the beam hits the SLM in a small angle the diffracted orders will be focused on a RGB camera. Another possibility would be to project the content on a screen with magnification optics, instead of the CCD.

Below we show a breadboard demonstrator setup with a REALHOLO chip installed. But for the investigations it was also used with other types of SLM from HOLOEYE and TI. Work with the PHS prepared it to accommodate the REALHOLO AHS as well.

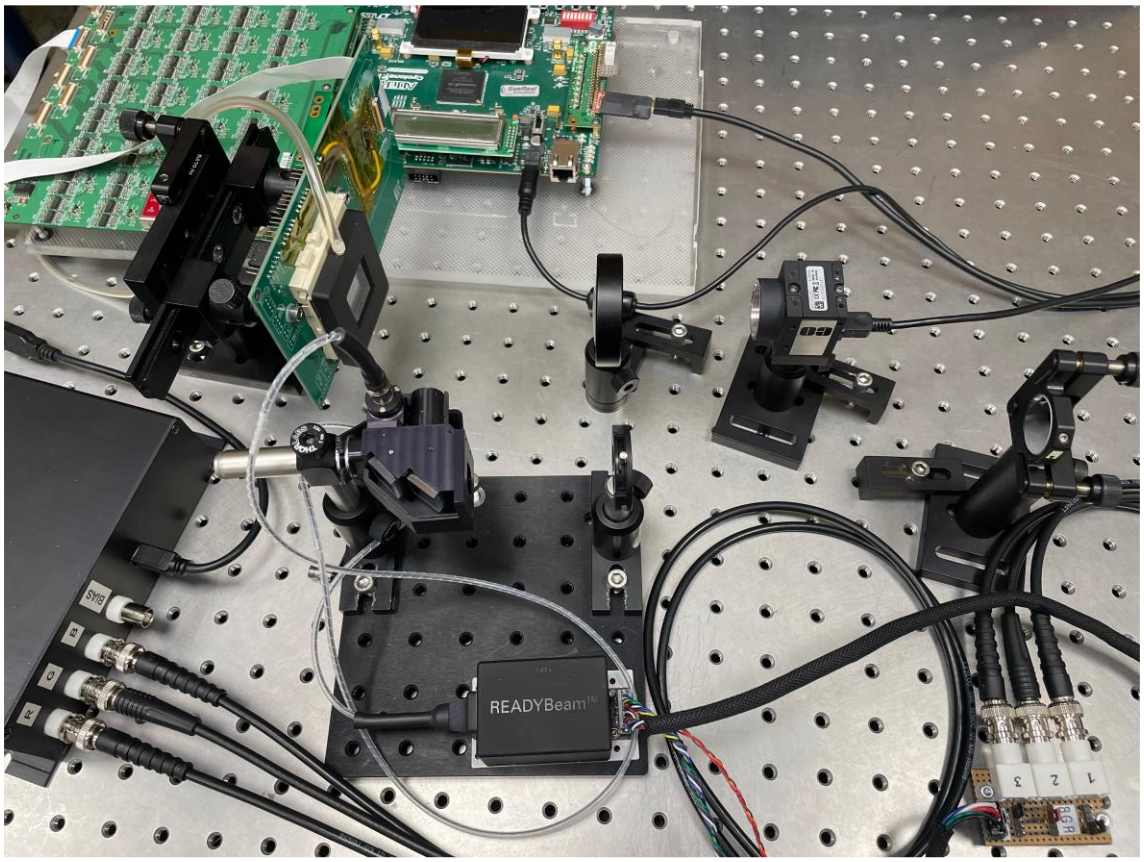

Figure 27: Potential breadboard projection demonstrator with REALHOLO chip.

3.5.2 Monochrome CGH

HOLOEYE’s standard for CGH computation has been focused on 8-bit depth in most cases. This is because of the consumer standard for most displays. On the other hand we have an internally developed software *qDOE* which is used for very sophisticated computations of diffractive optical elements (DOE). Due to the high flexibility in the design and fabrication of DOEs, the design space is much more open than it would have to be for SLMs, e.g. with their fixed pixel pitch in a given device. For this project we adapted *qDOE* to fit the requirements of the various SLM types. We used a method where hologram tiles, which later are replicated to fill the SLM surface, are calculated on the principle of iterative Fourier transform algorithm (IFTA), also known as Gerchberg Saxton algorithm.

For use with TI hardware, first the available bit depth was limited to 4bit. Second according to its total resolution, a tile size was defined, balancing e.g. the number of tiles, the number of iterations and the boundary conditions of reconstruction in the far field. In this example we settled on a diffraction angle of 2° with a content size of 200x200. Resulting in a tile size of 341 in x and 329 in y for the red laser source at 660 nm.

In addition to adapting the bit depth of the CGH, we also implemented a mask as boundary condition to define an area of interest (AOI) on top of the content. Standard calculations often use the full available pixel array for hologram encoding. This has impact on hologram computation and on reconstruction (image) quality. Introducing an AOI on the hologram generates additional freedom for CGH. The AOI may be surrounded by a frame-shaped “don’t care”-area into which, as part of the diffraction-based computation, light can be diffracted which does not contribute constructively to the image. In our example, we define an AOI region in which dark regions, where the reconstruction shall be black with good contrast, are higher weighted during the computational iterations.

An exemplary test of this CGH computation principle was done with the TI PLM for various weightings/levels of noise reduction. The camera is kept at the same settings throughout the image series. In Figure 28 one can see that the black area becomes noticeably darker. A similar effect can be noted for the first order, slightly decreasing as well. Nonetheless we expect a much bigger contrast improvement for CGHs with higher bit depth as will be provided by REALHOLO AHS.

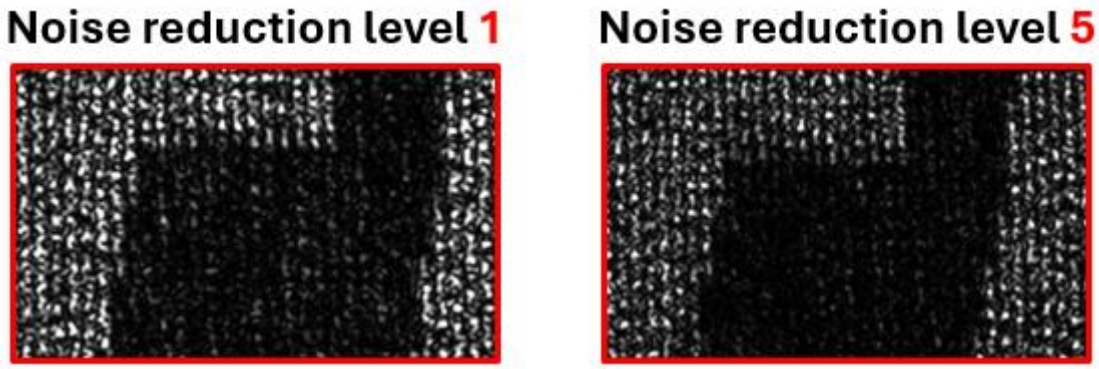

Figure 28: CGH reconstruction with camera. Noise reduction level 1 vs 5.

3.5.3 Colour CGH - CFS

For the CFS reconstruction we triggered the RGB laser in fast colour mode. Since the diffraction angle at given tile size is wavelength depended, we compute dedicated CGHs for each colour. Meaning, we have to match diffraction angles by varying the pixel tile size. Smaller tiles for blue light and larger tiles for red. As seen in Figure 29, imperfect tile size is visible in projection. An offset can be used to compensate potential deviations resulting from computation artifacts or the optical system.

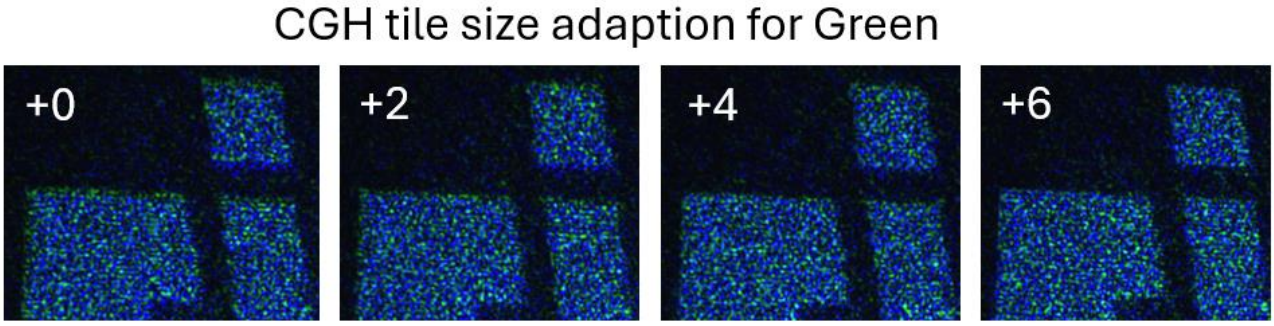

Figure 29: Effect of hologram tile size variation on precision of colour super-position.

The proper number of pixels for the tiles is shown in Table 1.

Wavelength	initial pixel_num_set X	Initial pixel_num_set Y	matched pixel_num_set X	matched pixel_num_set Y
660 nm	341	329	**337**	**325**
520 nm	269	259	**275**	**265**
450 nm	233	225	**233**	**225**

Table 1: Tile size given by pixel number in X and Y direction for different wavelengths. Initial calculation versus finalised colour matched parameters.

This approach can also take into account rectangular shaped pixel like the ones from REALHOLO which also alters the diffraction angle between X and Y orientation. We use these values for investigations of full-colour laser speckle effects in the next chapter.

3.5.4 Despeckle

The high frame rate of the MEMS-SLM can be used for averaging the intensity noise pattern (speckle) from undesired interference effects. One solution is varying the start phase for calculation of the holograms of each sub-frame which in turn leads to a different speckle pattern when reconstructing the hologram into an intensity pattern, our image. When projecting these sub-frames, which contain the same image content but a different speckle pattern, the speckle noise is averaged and therefore the speckle contrast is reduced, resulting in smooth texture of the image. It should be noted that the resolution of the camera for the pictures below is better than the human eye at that distance; therefore speckle contrast looks better to the eye at actual use.

This is only one of many ways to utilize the high frame rates of MEMS-SLMs, but it is quite an effective example to show in a demo.

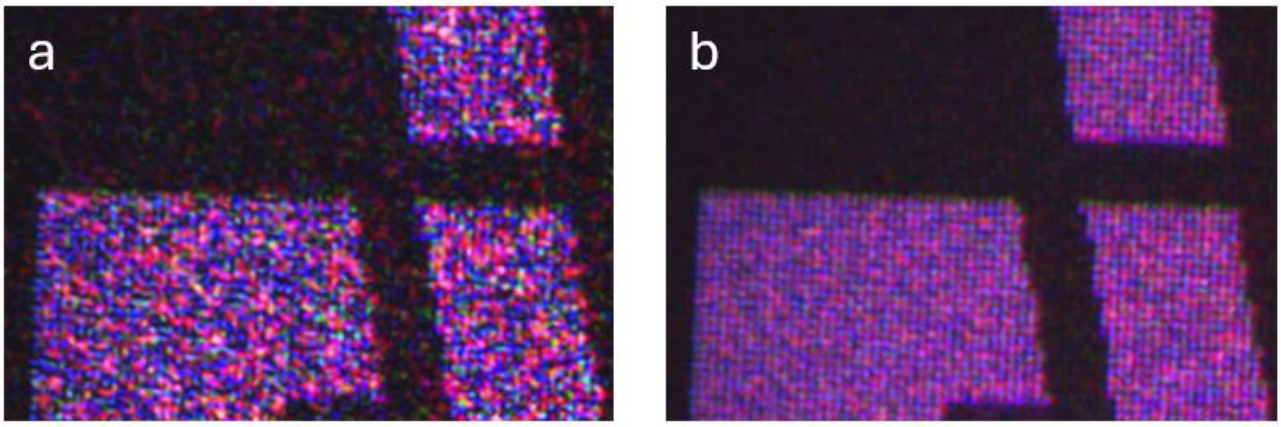

Figure 30: Captured image of CFS reconstruction with long exposure time. Initial phase constant (a) and 8 different initial phases alternated (b).

Chapter 4 Diffractive Projection Engine (DPE)

After successfully testing the laboratory projection setup demonstrator and being able to determine the phase-modulator performance, a further degree of integration is realized. In this chapter, we describe the optical and mechanical design of a small and modular diffractive projection engine (DPE), which is intended to be used as a demonstrator for structured illumination.

Independent of hardware availability, optical, mechanical and electrical compatibility of designs can be prepared and validated. Work with substitute hardware is done for development and validation of test systems and methods. On the other hand, design data in combination with existing component hardware is used for preparation of future system integration of REALHOLO components with potential test setups or use cases.

While we are aware that designs will greatly change in future iterations, principle compatibility still is of importance and intermediate solutions contribute to de-risking and acceleration of future iterations.

The first part of this chapter (4.1) describes the design of an existing DPE and its shortcomings in regards to the REALHOLO AHS (chapter 4.1.1). Adaptions, optical (chapter 4.1.2) and mechanical (chapter 4.1.3), are described for our focus on creating a robust optical system that integrates seamlessly with MEMS based AHS technology. In chapter 4.1.44.1.4, the developed alignment and test pattern, essential for precise measurements on full-colour diffractive systems, is presented. This is followed by a discussion of innovative methods for speckle reduction, ensuring optimal performance in structured illumination applications (see chapter 4.2).

4.1 Optical and mechanical design of DPE

The blueprint for the project's compact optical engine is a previous system design from HOLOEYE, called Diffractive Projection Engine (DPE). A DPE-variant, tailored to use selected aspects of LCoS-SLM with a given specification, already existed before HOLOEYE stepped into the project, replacing SeeReal and taking over important aspects for validation of the new technology as well as for introducing it to suitable high-value markets.

Key parameters of the optical system are shown in Table 2.

Parameter	Value
Magnification	Nominal 5.1x @520 nm (R: 4.97x, G: 5.1x, B: 5.2x)
Minimal Working Distance	0.2 m
Focus Distance	Afocal System
Size	35 mm x 65 mm x 50 mm
Light Source	Single mode fibre (FC/APC)

Table 2: Optical and mechanical parameters of the compact diffractive projection engine.

As shown in Figure 31, light gets coupled into the system from a single-mode fibre at the lower right and gets collimated by an achromatic lens doublet. A folding mirror directs the expanded beam onto the SLM (top), where it gets modulated and reflected towards the next folding mirror. The beam then passes through the optical system, basically a telescope, to the right, where it gets magnified and focused.

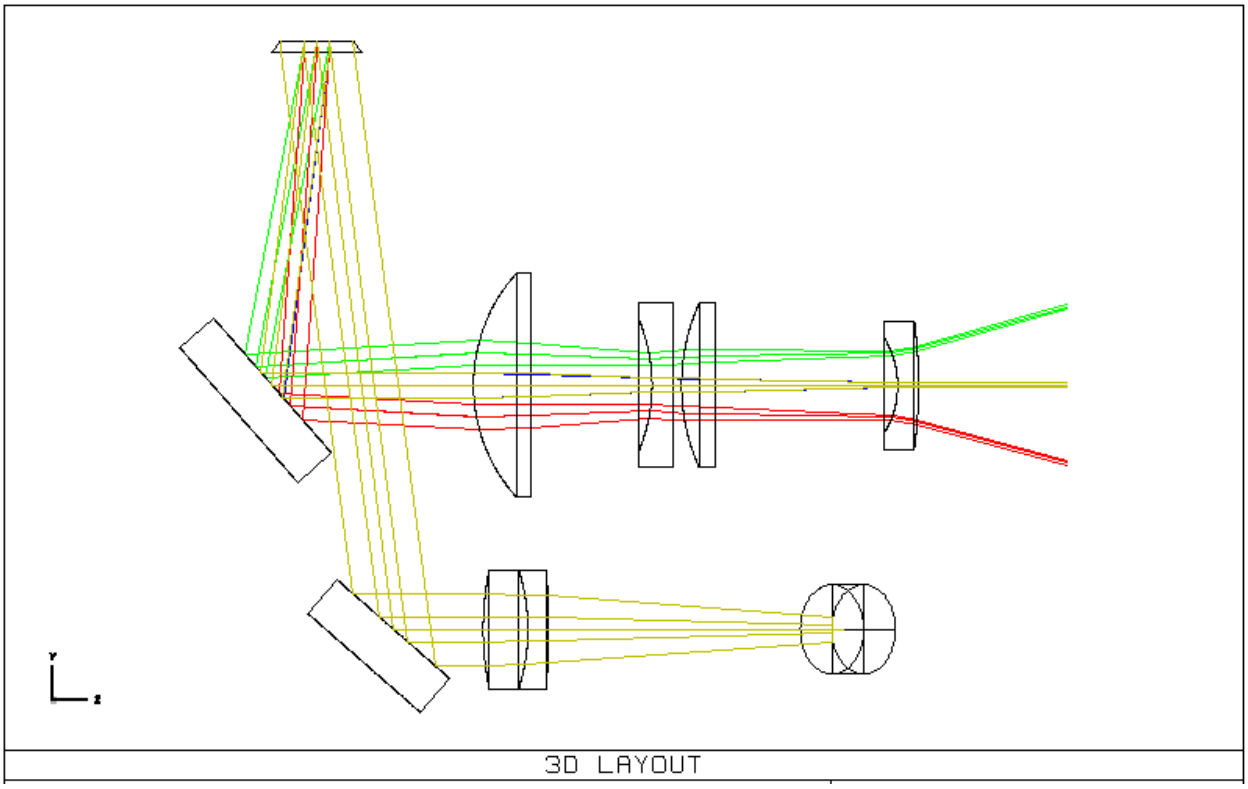

Figure 31: Schematic layout of the DPEs optical system.

It is important to note here, that the system is afocal, works for the whole visual range of the spectrum, provides a 5x magnification and is fairly compact and modular (see Figure 32).

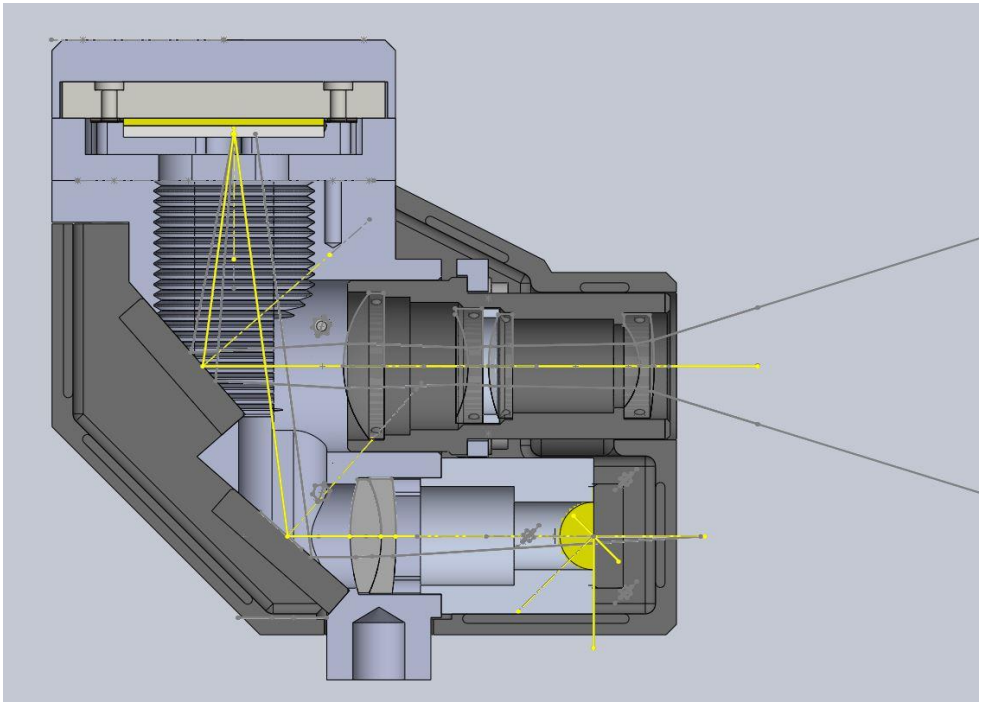

Figure 32: Cross-sectional view of the DPE including mechanics and housing as used for measurements with LCoS SLMs.

The DPE is especially useful in a fringe projection system as it allows for a large working area (or region of interest) at a short distance, due to it's 5x magnification. In addition, as the system is afocal, there's no need for an active refocusing mechanism.

As the system works by diffractive image generation, it is possible to correct for image aberrations, which is one of the typical use-cases for phase-modulating SLMs. The correction can be performed individually for each wavelength as the content is addressed sequentially and the SLM gets illuminated by defined light pulses. As noted in Table 2, the DPE shows a different magnification for each wavelength. To compensate for this, correction factors have been calculated, that are applied to resize the CGH structures on the SLM and therefore change the diffraction angle defined by the size of the addressed structures. The correction factors are as follows:

- R: 0.975
- G: 1.0
- B: 1.02

4.1.1 Limitations of existing DPE

For a central beam passing through the optical system, the following optical path differences and spot are calculated (see Figure 33).

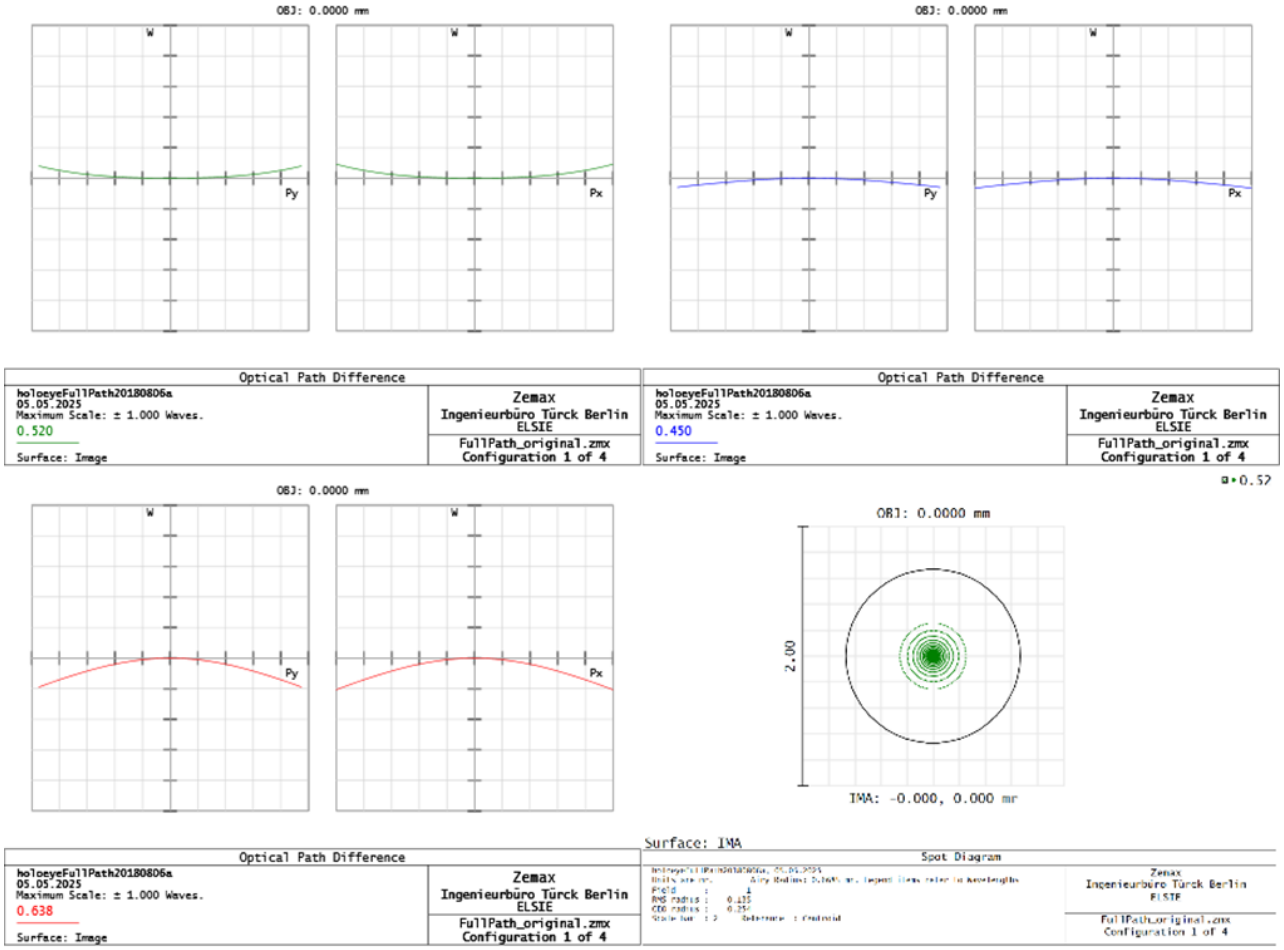

Figure 33: On-axis performance (optical path difference) of DPE at 520 nm, 450 nm and 638 nm wavelength.

The spot-size is well below the diffraction limit as can be seen in the spot diagram. Also, the optical path difference (OPD) is very low and below one lambda for 450 nm, 520 nm and 638 nm.

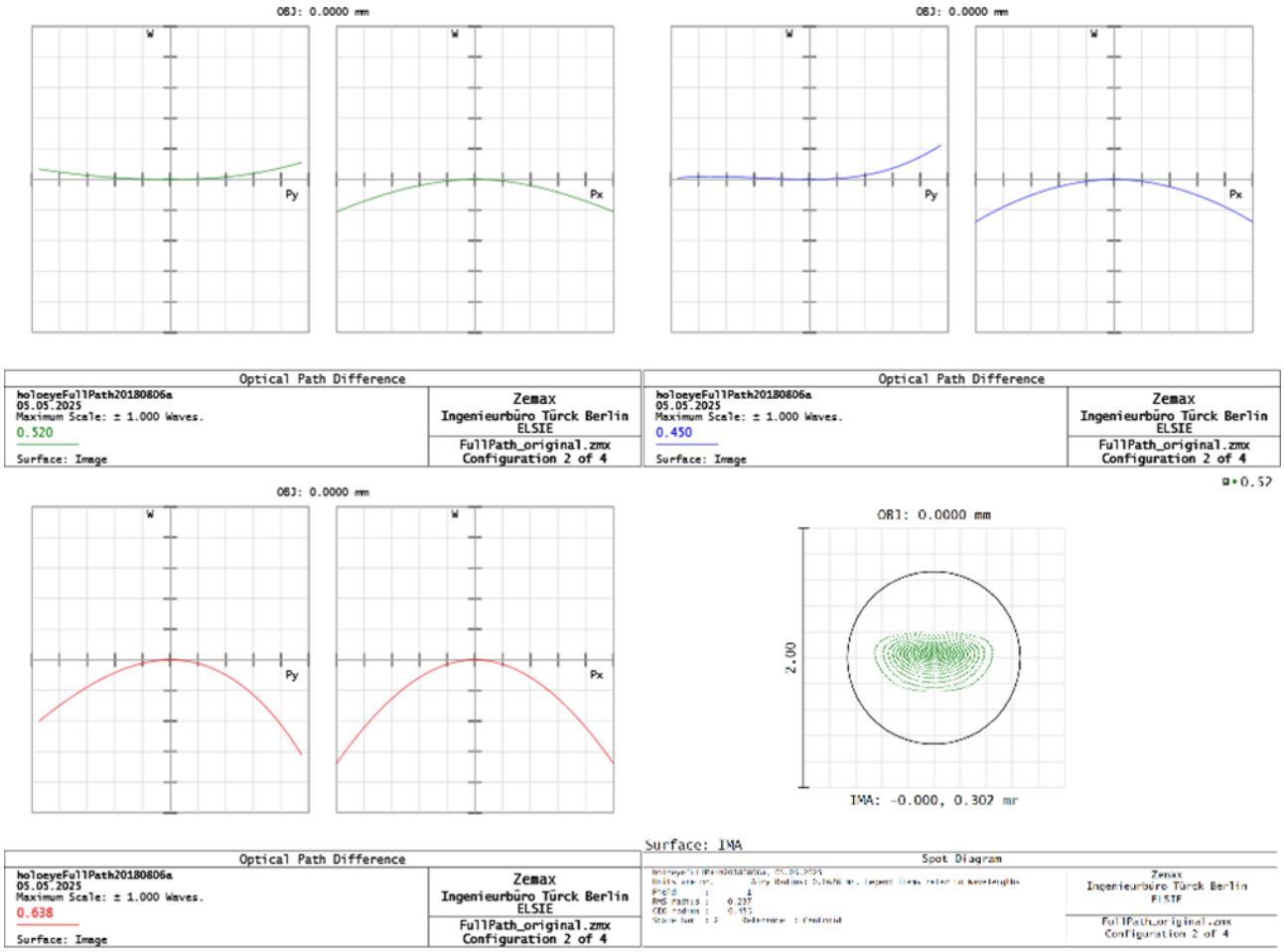

Figure 34: Optical path difference of DPE at maximum diffraction angle with pixel size of 4.5 µm for 450 nm, 520 nm and 638 nm wavelength.

For the case of the maximum diffraction angle of 3.3°, which corresponds to a pixel size of 4.5 µm, the spot sizes and OPDs still look acceptable (see Figure 34). However, one needs to keep in mind, that these are ideal numbers without any pointing errors from assembly or mounting the illuminating fibre or the SLM.

As the existing DPE wasn't specifically designed for the AHS, there is no margin left for the AHS. The main problem is, that the original design was optimized for an LCoS SLM with a pixel-size of 4.5 µm. As discussed in chapter 3.2, the full diffraction angle is usually not used in an LCoS based system due to pixel cross-talk and therefore a significant loss of diffraction efficiency for very fine structures.

When applying the actual AHS pixel size of 4 µm x 6 µm and applying some additional margin, vignetting and smeared spots can be seen in the simulation (Figure 35).

The following configurations are shown:

- Conf1 = on-axis = 0°
- Conf2 = off-axis with 111 LP/mm = 4.5 µm Pixel = 3.3°
- Conf3 = off-axis with 166 LP/mm = 3.0 µm Pixel = 5°

For a wavelength of 638 nm at 3.3°, the spot is already larger than the diffraction limit. Even worse, at 5°, vignetting appears (as can be seen in Figure 36). It is therefore necessary to perform a redesign of the optical system.

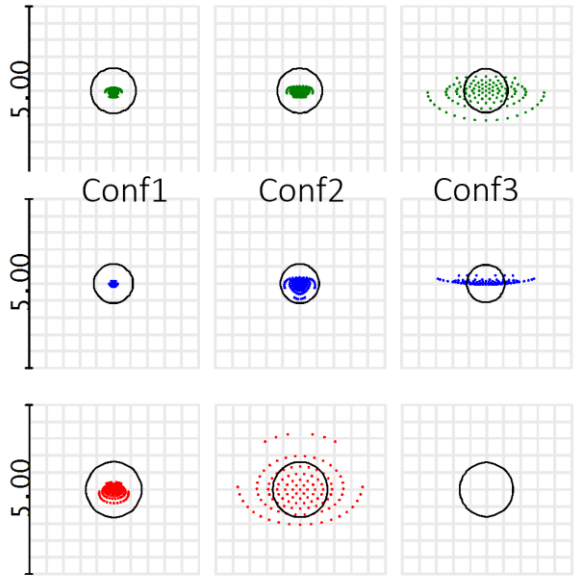

Figure 35: Spot-sizes of existing DPE on axis (Conf1), with 4.5 µm pixel size (Conf2) and 3.0 µm pixel size (Conf3).

4.1.2 Adaption of optical design for REALHOLO AHS

Based on the known limitations of the DPE mentioned above, a new optical system has been designed. The target is to increase the maximum allowed angle to 5°. This value corresponds to the maximum diffraction angle at a pixel size of 3 µm, which is smaller than the REALHOLO AHS pixel and therefore leaves some margin for pointing errors in the assembly and mounting process. A second target is to reduce the system complexity and use, if feasible, off-the-shelf standard optical components to reduce costs, risks in production and lead-time.

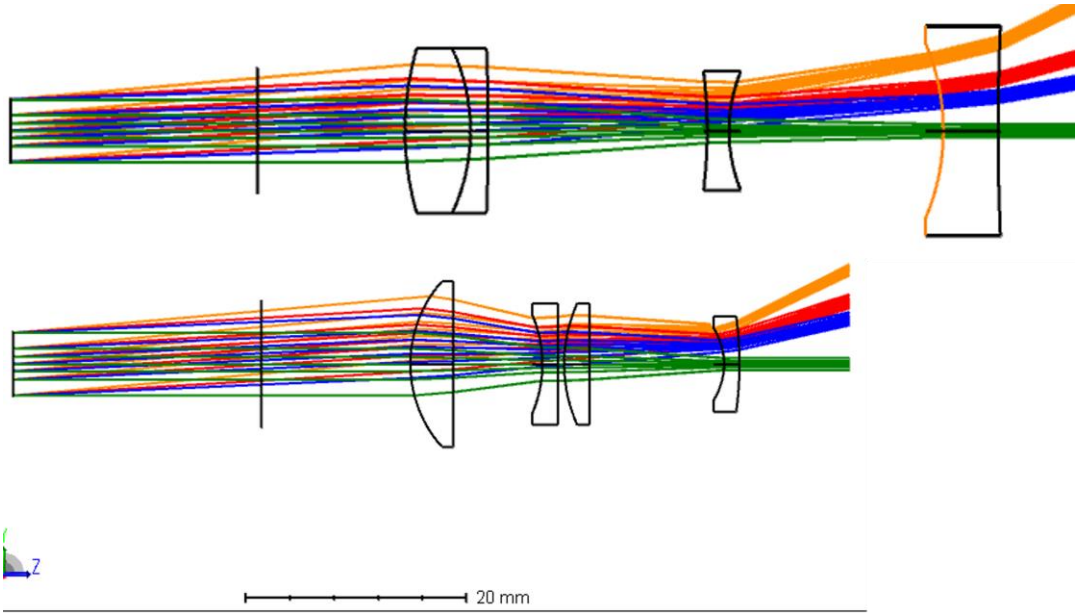

Figure 36: Size comparison of existing DPE (bottom) and new design (top).

The result of the design process is shown in Figure 36 at the top. The system has been reduced from 4 optical elements to only 3 elements. The first element, a doublet, is a standard lens from Edmund Optics, while the two concave lenses are still custom designs. As one can clearly see, the beams at 5° (indicated in orange) are now no longer vignetted by the last element. On the downside,

the length from the first lens to the last surface has increased by almost 100% and the diameter of the last element also increased significantly, which would result in a larger engine.

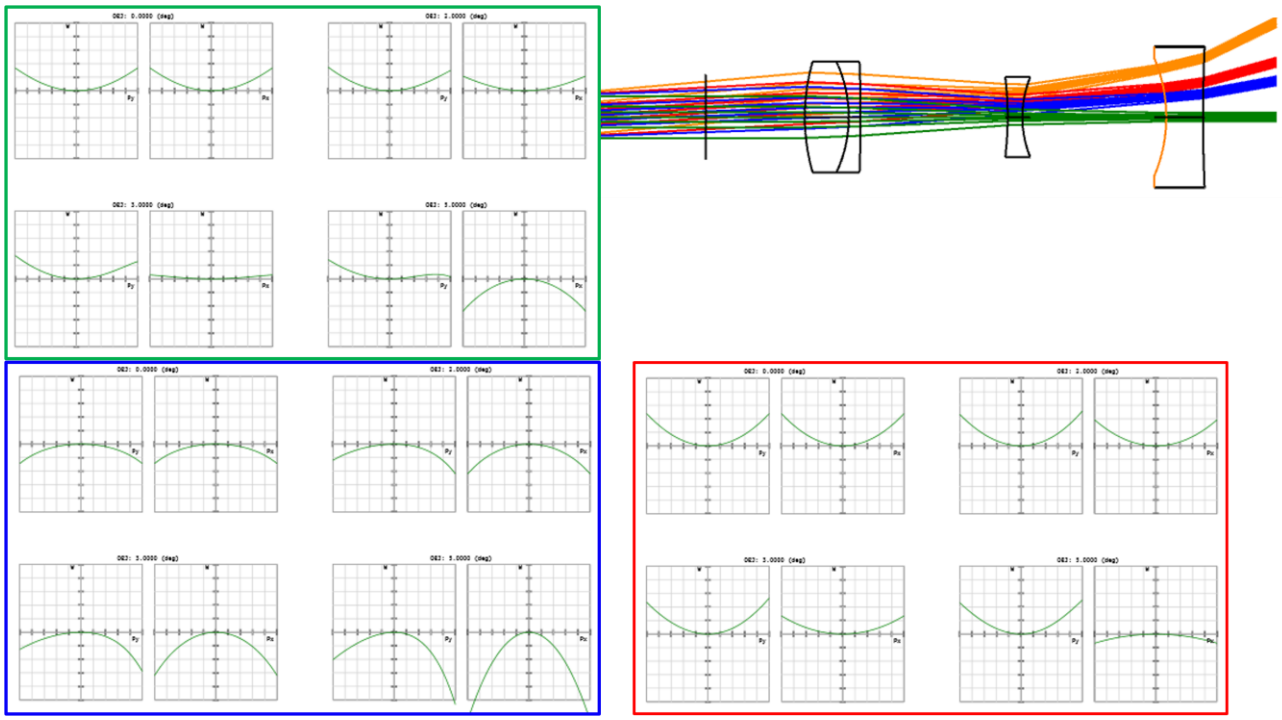

Figure 37: Optical path difference of new optical design for 0°, 2°, 3° and 5° at 450 nm, 520 nm and 638 nm wavelength each. Maximum scale ±1 waves.

As shown in Figure 37 and Figure 38, the new designed optical system is almost diffraction limited for the whole intended spectrum (450 nm to 638 nm) and the maximum angle of 5°. Also the optical path difference remains below one lambda in most cases. The extreme combination of 450 nm and full angle of 5° is an exemption with slightly larger spot-size and optical path difference.

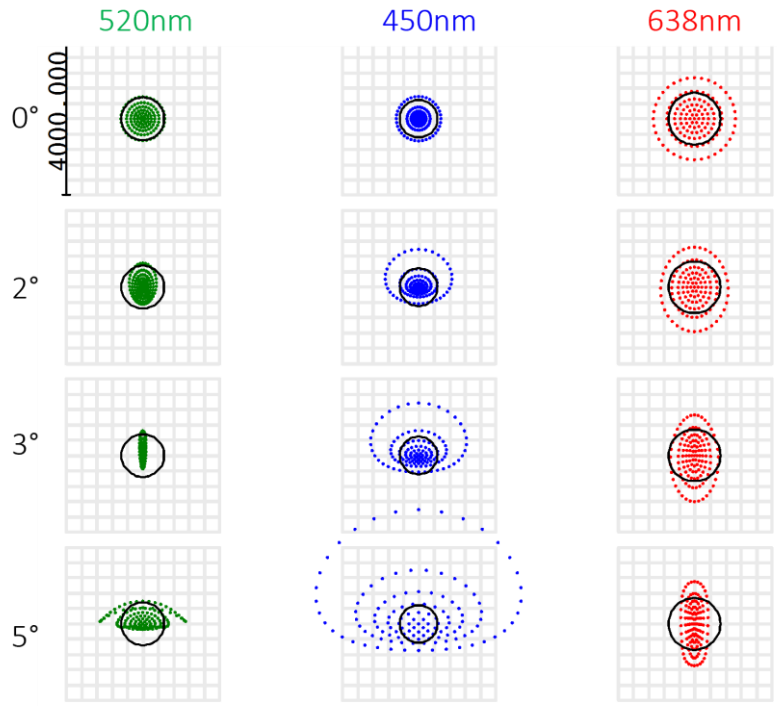

Figure 38: Spot diagrams for different diffraction angles and wavelengths. The black circle indicates the diffraction limit of the system.

Based on the outcome of the optical design process, a decision has been made to first keep using the existing optical system as it is smaller and real-world performance has to be tested with AHS. Switching to the new design at this stage of the project without available AHS, doesn't justify the potential risks of manufacturing and assembling the new design.

4.1.3 Adaption of mechanical design for REALHOLO AHS

Below in Figure 39, it is shown, how a compact DPE can be combined with the REALHOLO AHS. This investigation does not only consider mechanical restrictions, but more importantly, optical parameters as distance between image planes and alignment tolerances.

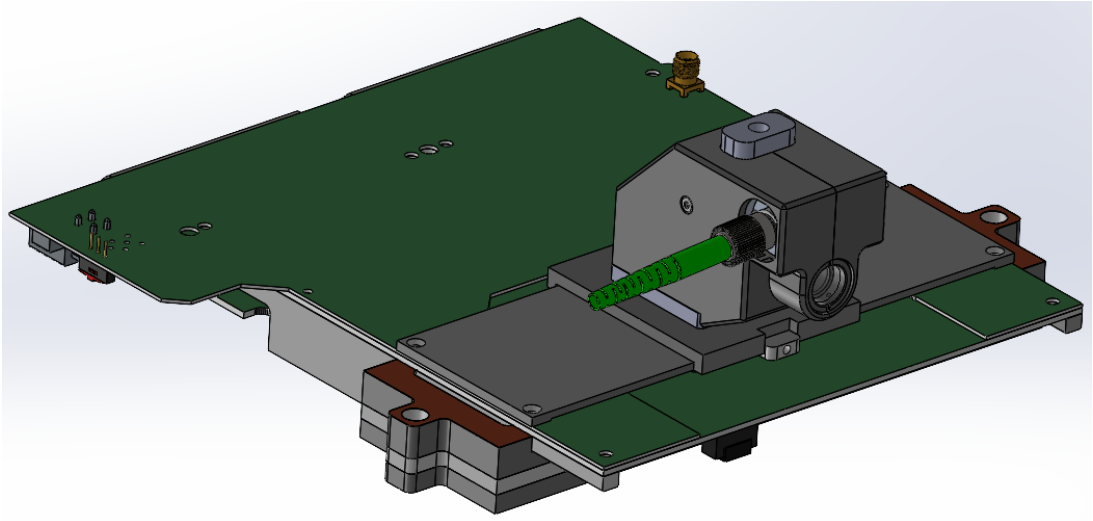

Figure 39: Isometric view of DPE mounted on AHS driver-board.

The adapter is designed in a way, that a necessary nitrogen purge as well as a protecting cover-glass are implemented. Apart from a possible extra reflection from the additional cover-glass, we don't expect any negative influence on the DPE performance.

Figure 40: DPE with attached adapter for mounting on AHS. Left: isometric top-view. Right: Front-view of DPE (top-down). The FC-APC fibre adapter is visible on the left side of the DPE.

Figure 40 shows photos of the DPE including the designed and manufactured adapter to mount it on the AHS driver board.

4.1.4 Alignment- and Test-Pattern

As already performed manually in chapter 3.5.3 without a defined test pattern, it is necessary to align the three colour images after they passed through the DPE. Furthermore, a test pattern is needed to be able to easily perform measurements to evaluate the generated structured illumination.

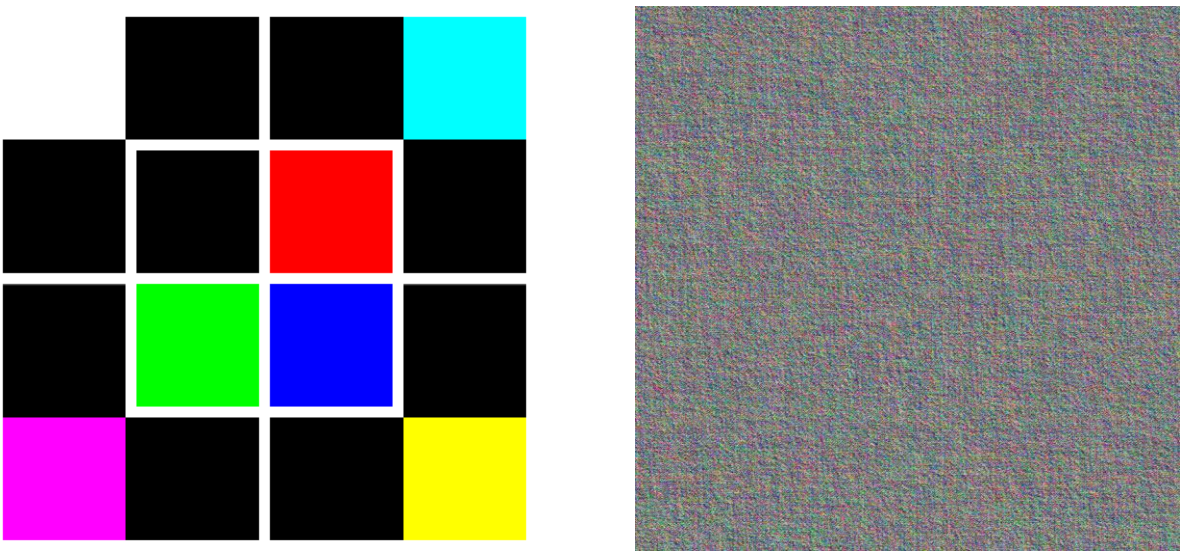

Figure 41: Developed target pattern (left) with the calculated CGH (right).

As a consequence, a custom test-pattern has been designed and calculated as a CGH (see Figure 41). It is designed to facilitate precise alignment, colour-mixing, contrast evaluation, and distortion correction in optical systems. Below are the key features of the test pattern:

- Black areas
  - The pattern includes extensive black regions, which are essential for assessing contrast and ensuring accurate alignment in the setup.
- White area
  - A dedicated white area is incorporated to enable contrast measurement and serves as a reference for colour mixing. This area is crucial for evaluating the performance of the optical system in reproducing accurate colours.
- RGB areas
  - The test pattern features distinct RGB sections, which are used to determine colour coordinates within the CIE 1931 colour space. These areas are vital for calibrating colour accuracy and ensuring consistent colour reproduction.
- Cross-bar and straight white lines
  - These elements are included to address distortion and magnification correction. The cross-bar and straight lines help in identifying and correcting any optical distortions present in the system.
- Equal colour components
  - All colour components are presented with equal intensity, which is critical in diffractive setups where light is redistributed. This ensures that the test pattern provides a balanced and accurate representation of colours.

4.2 Despeckle with low computational effort

As already discussed in chapter 3.5, speckle in laser-based systems can pose a significant challenge, as it can significantly degrade image quality. We explore advanced techniques for real-time CGH calculation, emphasizing efficient speckle reduction methods. By leveraging spatial light modulators and innovative algorithms, we aim to enhance image clarity and resolution, paving the way for improved holographic applications.

Real-time CGH calculation is possible on standard computer hardware, including a normal GPU, based on Gerchberg-Saxton algorithm (IFTA), as explained in chapter 3.5.2, and accelerated on a GPU. However, the input image resolution and the calculation frame-rate is limited. For a real-time application with despeckling, it is not possible, or at least not feasible, to calculate multiple CGHs with the same input signal to achieve time-averaging, as has been used in chapter 3.5.4.

To overcome this limitation in REALHOLO, we focus on a time averaging method with CGHs that are only shifted spatially instead of calculated multiple times. The underlaying concept has been first presented in 2009 by L. Golan and S. Shoham: "Speckle elimination using shift-averaging in high-rate holographic projection" [2] and is described in the following section.

4.2.1 Golan/Shoham

Multiple methods exist to reduce speckle:

- Time averaging of multiple calculated CGHs
  - High computational cost
- Time averaging by random shift-averaging of the same CGH
  - Low computational effort but limited performance
- Time averaging by defined shift-averaging of the same CGH
  - Low computational effort with best despeckle performance

All of the aforementioned methods rely on time averaging. In case of image reconstruction for the human eye, the averaging time needs to be faster or equal to 60 Hz. In case of a camera-based system, e.g. for fringe projection, the sensors shutter speed is the limiting factor.

The method of Golan/Shohams is as follows:

1. Calculate CGH with a tile-size of N x M pixels
2. Address the same CGH with spatial shifts based on factor c
   a. The number of addressed frames per CGH is c^2
   b. Raster the CGH in steps of N / c and M / c with one addressed frame per position
3. Integrate with the used sensor of a duration of c^2 frames, synced to the change of the input CGH

The process of rastering the CGH can be performed with very low computational effort, as the CGH in the GPUs memory only needs to be cyclically shifted by a defined amount of pixels.

In addition to the original publication from Golan/Shoham, which makes use of a fast binary switching FLCoS SLM, an additional work by Parry et al. ("Application of a liquid crystal spatial light modulator to laser marking", 2011) [3] uses the same method for laser marking, which makes it a well documented method that has already been tested in two different fields.

Expected improvements as demonstrated before by Parry et al. are shown in Figure 42 and Figure 43.

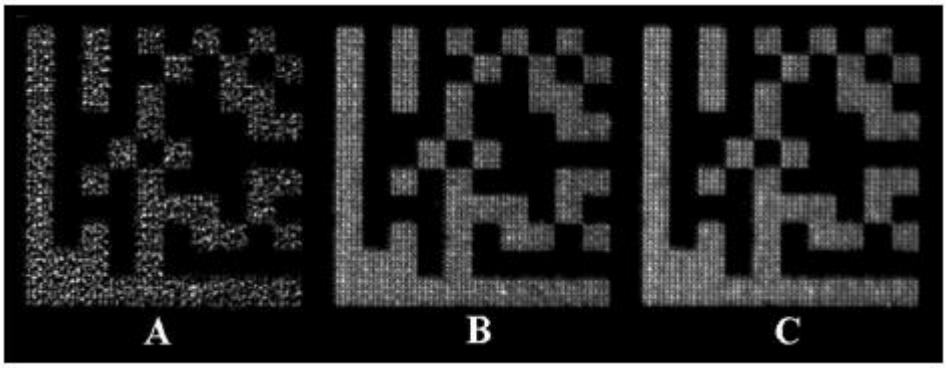

Figure 42: Images of holograms with A) a single CGH, B) 16 random spatial shifts, C) 16 defined spatial shifts; all combined and normalized in software. Work performed by Parry et. al. [3].

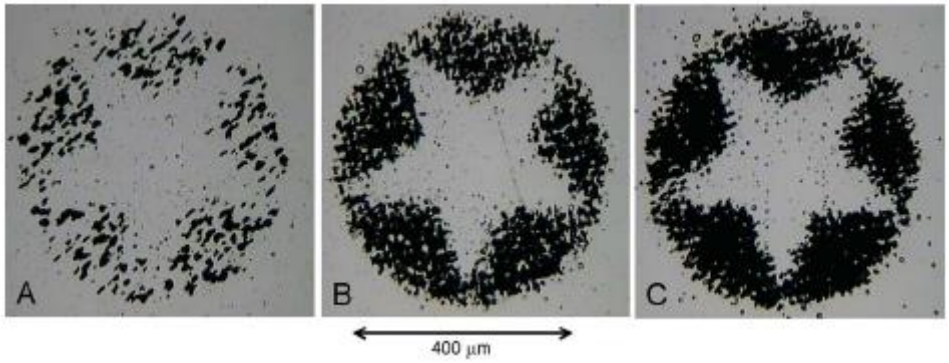

Figure 43: Images of marks on a thin layer of aluminium coated glass created with an SLM and calculated CGHs with 200 ms exposure each. A) a single CGH, B) 16 random spatial shifts, C) 16 defined spatial shifts. Work performed by Parry et. al. [3].

4.2.2 Results with HOLOEYE LETO-720 LCoS SLM

Due to the fact, that no REALHOLO AHS was available until the preparation of this report, a test setup with alternative hardware was used to test the method from Golan/Shoham.

Instead of the MEMS AHS, the fastest available HOLOEYE LCoS SLM was chosen, modified and integrated into the test setup. Starting point is a LETO-3-VIS-127-CFS with a fast switching display for the visible range, optimized for CFS image reconstruction at room temperature. The SLM works with a full-colour (RGB888) input image at 60 fps. The image data is sequentially addressed on the SLM at a modulation field-rate of 180 Hz. The combined response-time of the SLM (10%-90% rise + 90%-10% fall) is below 2 ms at room temperature. However, this is still too slow for a meaningful despeckling process, which requires 9 fields or more at the integration time of the human eye (60 Hz). In order to increase the switching speed, two factors have been modified. First, the display temperature has been increase to ~55°C, which decreases the LCs rotational viscosity and therefore decreases especially the fall-time. Second, a different set of driving voltages with higher offset-voltage has been used, which reduces the rise-time.

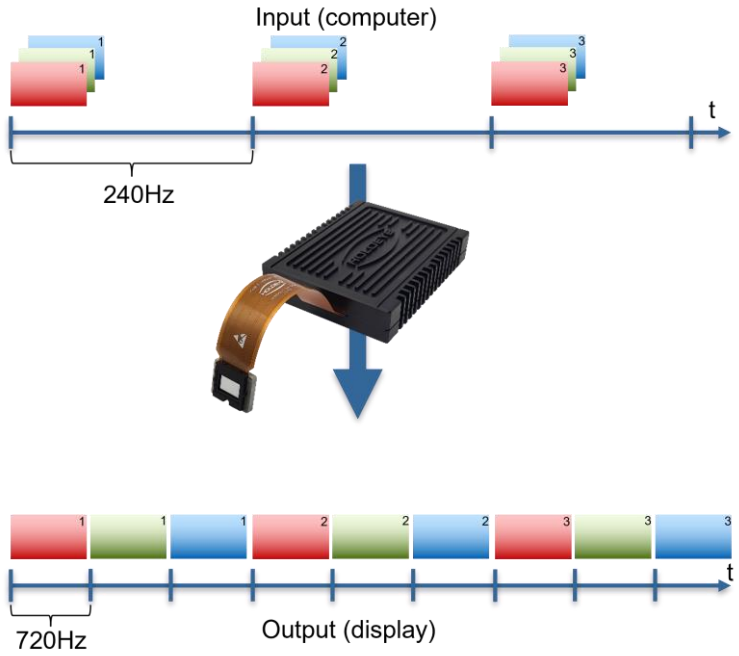

Figure 44: LETO-720 diagram showing the conversion from 240fps full-colour RGB888 to 720 Hz monochrome modulation.

In addition to the electro-optical changes, a different display driver with higher bandwidth has been adapted to support a higher frame-rate. The SLM now operates at 240 fps with RGB888 input signal. By encoding different CGHs into the three colour channels, the modulation rate can be further increased by a factor of 3 from 240 Hz to 720 Hz, see Figure 44. The LCoS SLM is called LETO-720 and its parameters compared to the REALHOLO AHS are shown in Table 3.

Parameter	REALHOLO AHS	HOLOEYE LETO-720
Modulator	MEMS (Analogue Modulation)	Liquid Crystal (Digital Modulation)
Pixel Size	4 µm x 6 µm	6.4 µm x 6.4 µm
Resolution	4000 x 2048	1920 x 1080
Phase-Resolution	8-Bit (10-Bit mode avail.)	4-Bit
Response-Time	~35 µs (< 5µs tested)	<1 ms
Modulation Rate	>1 kHz	720 Hz
Wavelength	RGB CFS	Monochrome

Table 3: Comparison of REALHOLO AHS with HOLOEYE LETO-720.

In regards to the despeckling capabilities, LETO-720 has several limitations, which show the expected advantage of REALHOLO AHS. The key parameter for despeckling is the response-time of the SLM in combination with the phase-resolution and the modulation rate. Even though LETO-720 is a very fast modulating SLM compared to other LCoS based phase-only modulators, the response-time is more than a magnitude slower than REALHOLO AHS. Instead of using a c-factor of 4 (16 spatial CGH shifts in one integration period of the sensor), as planned with AHS, only a c-factor of 3 could be realized with the LCoS SLM. The phase-resolution is limited to 4-Bit and it can only operate with a monochrome light source. Due to the digital modulation, temporal fluctuations of the phase modulation are present (flicker), which together with inter-pixel crosstalk lead to a degradation of the diffraction efficiency and increase the background noise.

The following setup, as shown in Figure 45 has been realized: A HOLOEYE LETO-720 display is mounted in a DPE system, which is supplemented with a TEC on top to keep the target panel temperature at around 55°C. A polarization-maintaining single-mode fibre is attached to the system, to illuminate the SLM at a wavelength of 520 nm. Depending on the measurement, either a camera is placed a few centimetres behind the optical system (cropped images of the addressed content), or a screen is placed at a distance of around 0.3 m.

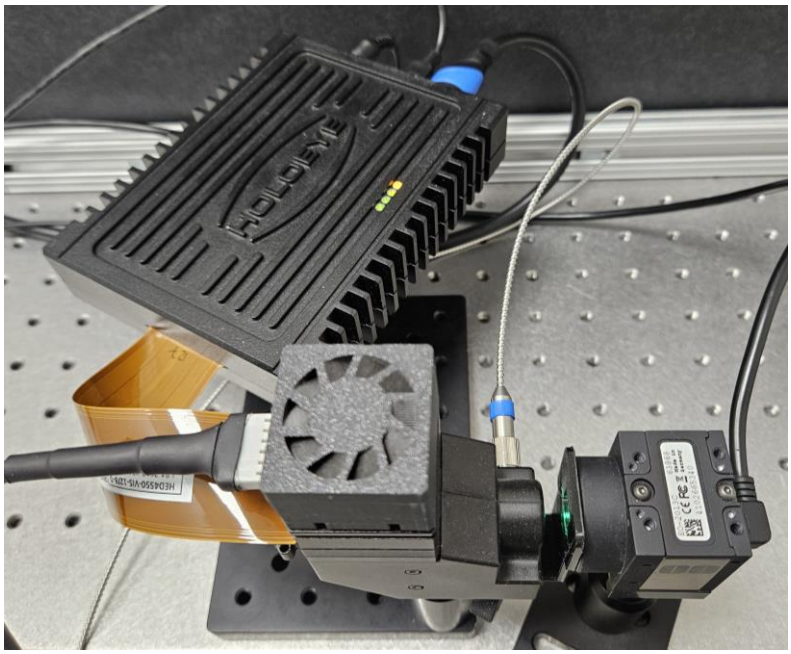

Figure 45: Test setup of a HOLOEYE LETO-720 inside a DPE with TEC on top. Light is incoupled via a polarization-maintaining single-mode fibre. The camera is placed directly behind the DPE.

An example photo of content visible on the screen can be seen in Figure 46. Please note, that the vertical line of small dots is not part of the intended image, but rather generated by horizontal addressing artefacts on the SLM.

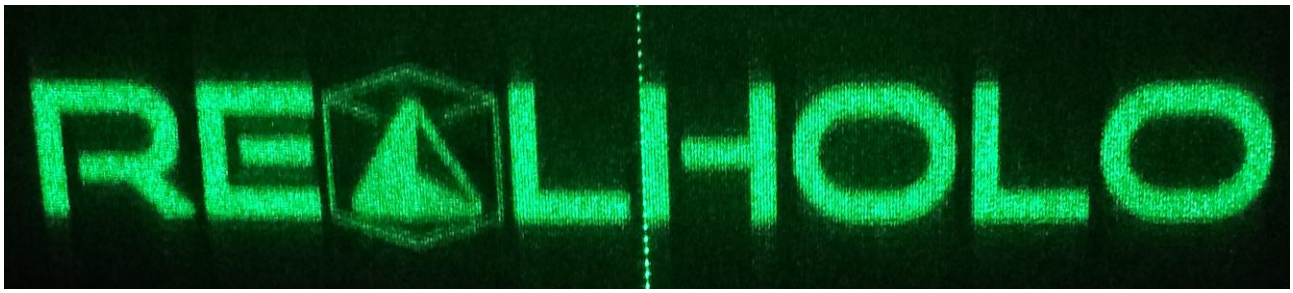

Figure 46: Photo of REALHOLO logo, generated by a HOLOEYE LETO-720 inside a DPE.

As can be seen in Figure 47, the effect of despeckling on image quality is significant. Please note, that the images are taken at a wavelength of 520 nm behind the DPE's magnification optics and directly onto a monochrome camera chip. A Fresnel-lens function was superimposed onto the CGH to adjust the focus, which increases the spatial frequencies, that need to be addressed onto the SLM and therefore also reduce the image quality.

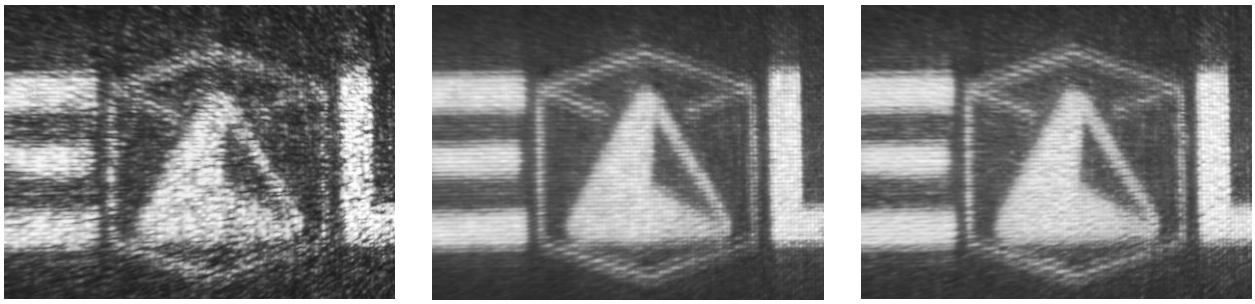

Figure 47: Cropped image of the REALHOLO logo after DPE, directly on camera sensor. Left: Single calculated CGH. Middle: 9 calculated CGHs. Right: Single CGH spatially shifted 9 times.

On the left, the result of a single calculated CGH can be seen, with a highly degraded image quality. The image in the middle shows the result of 9 individually calculated CGHs, that are addressed in one camera shutter period (1/80 s). Speckle is barely noticeable. An almost identical result can be seen in the right image. In this case, the Golan/Shoham algorithm with a c-factor of 3 has been applied to the CGH from the left image. A direct comparison between the images on the left and right, both taken at the same shutter speed and with almost the same computational effort, reveal the potential of this method. Further improvements are expected with the AHS due to the faster modulation speed, which results in an increase of c-factor and full colour modulation.

In addition, we expect even better image quality. Especially a better contrast value due to higher phase-resolution and no electrical pixel cross-talk, which is inherent to LCoS based SLMs.

Chapter 5 Summary and Conclusion

Development of setups for characterization and use of MEMS-based SLM was done from scratch and as adaptation of systems previously developed for LC-based devices. The preparation for high-speed measurements has been successful, involving hardware additions like an universal laser trigger box and high-speed RGB laser, and upgrades such as a high-speed line camera and software adaptations to integrate the new hardware and implement features as automated SLM control. Basic grating patterns were evaluated for the PHS chip, focusing on diffraction efficiency and verifying the phase response to achieve over 2Pi. Results showed minimal crosstalk for the REALHOLO MEMS, similar to a reference MEMS-SLM, the PLM from TI. While absolute values using PHS samples still exhibit some imperfections, they already show the great potential which will materialise with properly working AHS. Experience with LCOS characterization served as starting point for many measurements and as guidance for interpretation of MEMS results.

Identifying the PLM from Texas Instruments and integrating it in the plans, was additional effort but turned out to be a valuable addition to the development of tests. It could be used as a hardware substitute for time-resolved measurements and to demonstrate typical MEMS-SLM properties, including RGB capabilities. Using different types of phase modulating devices also motivated more advanced and more generic adaptation of HOLOEYE's CGH computation design space which is also very beneficial for work with future SLM variants. Future investigation is expected to include aspects as CGH, resolution of structured illumination, bit depth variation, noise reduction, despeckle, and RGB bit plane stacking. As fully functional AHS have become available recently, we are looking forward to continue our investigations (also) outside the scope of REALHOLO.

Progressing from investigations with the CFS lab demonstrator, we validate the abilities of a DPE and use it to demonstrate both the importance of proper system design for holography as well as the positive impact and potential of high-resolution, high-speed but low crosstalk phase modulation on key quality aspects of holographic image generation using the example of despeckle, one of the key inhibitors of laser-based systems.

While fully functional REALHOLO MEMS-SLM become practically available only very late in the project, using a high-speed LCoS with 720 Hz frame rate is quite suited as temporary substitute for system development and validation of key aspects of the future high-speed and high-resolution MEMS technology.

We can demonstrate the positive impact of high frame rates on visible quality but furthermore, we can highlight that the elimination of crosstalk in MEMS-SLM with high bit-depth will greatly improve effective spatial resolution and corresponding phase precision in individual pixels which in turn will amplify quality aspects as despeckle or holographic spatial resolution and contrast.

Future continuation of MEMS-SLM developments started with REALHOLO is expected to unlock the potential of the new technology platform for a wide range of applications, based on European supply chain contributors and IP.

Chapter 6 List of Abbreviations

Abbreviation	Translation
AHS	Active MEMS-SLM – fully functional SLM with MMA integrated with CMOS backplane to drive individual pixels according to a high-speed signal input
CCD	Charge-coupled device
CFS	Colour-field sequential – high-speed operation at multiple wavelengths which temporarily integrated to generate mixed colours, e.g. RGB-white
CGH	Computer-generated hologram
CW	Continuous wave
DE	Diffraction efficiency
DO	Diffraction order(s)
DOE	Diffractive optical element
DPE	Diffractive projection engine
FLCoS	Ferroelectric Liquid Crystal on Silicon
FPGA	Field-programmable gate array
GPU	Graphics Processing Unit
IFTA	Iterative Fourier transform algorithm
LC	Liquid crystal
LCoS	Liquid crystal on silicon
MMA	Multi-mirror array – pixelated array of electrically controllable mirrors
MEMS	Micro-Electromechanical System
OPD	Optical Path Difference
PHS	Passive MEMS-SLM – MMA with hardwired groups of pixel for characterisation and test purposes
PLM	Phase light modulator – used by Texas Instruments to differ between tilt and piston type MEMS-SLM
RGB	Red, Green, Blue – typical colour mix for display applications
ROI	Region of interest (here used for angular range of desired DO)
SLM	Spatial Light Modulator – Active pixel array for use in wavefront modulation or display applications, typically with coherent light
TGI	Twyman Green Interferometer
TI	Texas Instruments
WLI	White Light Interferometer

Chapter 7 Bibliography

[1] FISBA product webpage (https://www.fisba.com/en/readybeam)

[2] Lior Golan and Shy Shoham, "Speckle elimination using shift-averaging in high-rate holographic projection," Opt. Express 17, 1330-1339 (2009)

[3] Jonathan P. Parry, Rainer J. Beck, Jonathan D. Shephard, and Duncan P. Hand, "Application of a liquid crystal spatial light modulator to laser marking," Appl. Opt. 50, 1779-1785 (2011)